Fluorescence and ^{13}C NMR Determination of Side-Chain and Backbone Dynamics of Synthetic Melittin and Melittin Analogues in Isotropic Solvents†

Arthur J. Weaver,‡ Marvin D. Kemple,*,§ and Franklyn G. Prendergast*,‡

Department of Biochemistry and Molecular Biology, Mayo Foundation, Rochester, Minnesota 55905, and Department of Physics, Indiana University-Purdue University at Indianapolis, Indianapolis, Indiana 46205-2810

Received March 6, 1989; Revised Manuscript Received June 9, 1989

ABSTRACT: The dynamics in isotropic solvents of selectively ^{13}C labeled synthetic melittin and three analogues have been investigated by using NMR and fluorescence techniques both separately and in combination. In conjunction with the "model-free" approach to interpretation of NMR relaxation data [Lipari, G., & Szabo, A. (1982) *J. Am. Chem. Soc. 104*, 4546–4570], the availability of steady-state fluorescence anisotropy and lifetime data augment T_1,T_2, and NOE data to provide quantitative information about fluorophore dynamics in these peptides. A method is presented for using combined fluorescence and NMR data to obtain technique- and model-independent values for parameters describing local motion of ^{13}C-labeled fluorophores in peptides and proteins. The dynamics of melittin and melittin analogues are found to be consistent with structural characteristics inferred from CD, fluorescence, and NMR spectral information presented in the preceding paper (Weaver et al., 1989). In particular, the mobility of the random coil peptide monomers is shown to be quite similar, while side-chain as well as peptide backbone motion in the aggregated or oligomeric species differs markedly among the analogues. For melittin itself, experimentally determined overall rotational correlation times for the monomer and tetramer agree very well with values predicted on the basis of solvent-accessible protein surface area. The local dynamics of selectively ^{13}C-labeled Trp-19 and Gly-12 residues of melittin are also found to be consistent with peptide structure. In random coil melittin monomer, a specific model for the motion indicates that the Trp side chain moves through an approximate angle of ±71° about the β–γ bond with a correlation time of 159 ± 24 ps. In melittin tetramer, the indole moiety is spatially more confined with a flip angle of ±37°, yet demonstrates an *increased* rate of motion with a correlation time of 56 ± 8 ps. The constrained mobility of the Trp-19 side chain is consistent with motional constraints inferred from the X-ray structure of melittin tetramer. These results show that protein side-chain motion, even of moieties as large as indole, can occur on the picosecond time scale and that these motions are reasonably similar to those inferred from molecular dynamics simulations.

The advent of molecular dynamics simulations of biomolecule dynamics [for reviews, see Karplus and McCammon (1981) and Levy (1986)] has generated a need for experimental detection and quantitation of picosecond motions in macromolecules. This realization, taken with the likely significance of such motions to protein structure and function, provides ample justification for the development of experimental methods able to demonstrate the existence of, and to quantify the amplitude and time scale of, local motions in peptides and proteins. Recent publications demonstrate the usefulness of fluorescence (Petrich et al., 1987; MacKerell et al., 1987) and NMR (Weiner et al., 1987; Rice et al., 1987; Rule et al., 1987; Brown et al., 1988) spectroscopies for the study of internal motions in proteins. One limitation inherent in the application of these methods is the uncertainty regarding the accuracy of the experimental data when only one technique is employed. In principle, however, NMR and fluorescence can be used conjointly to study the dynamics of a fluorescent group in a macromolecule.

A major goal of this and previous work (Weaver et al., 1988) thus has been to *combine* fluorescence and NMR data for synthetic peptides containing a single tryptophan residue in an effort to generate a consistent description of side-chain motion. The feasibility of such an approach was demonstrated in an earlier study of tryptophan side-chain dynamics in two single-tryptophan hydrophobic oligopeptides (Weaver et al., 1988). In that as well as the present study, the approach was to incorporate tryptophan selectively labeled with ^{13}C at the $C\delta_1$ position (i.e., the 2-position) of the indole ring (Branchini et al., 1987) into the peptides by direct peptide synthesis. Although the earlier studies on hydrophobic oligopeptides demonstrated the general validity of the combined use of NMR and fluorescence data, confirmation of the applicability of this approach to more complex peptides and proteins is a logical second step. Specific aims of this work therefore included (a) the detection of local tryptophan side-chain and peptide backbone mobility in a variety of isotropic solvents, (b) the demonstration of a practical method for accurately quantifying picosecond motions in peptides and proteins using combined fluorescence and NMR data, and (c) the correlation of motional information collected for a set of peptide analogues with existing structural or dynamical data for the same or similar systems. The cytolytic peptide melittin provides a particularly useful and well-studied model for such investigations due to its diverse behavior in a variety of solvent environments.

In this work, the dynamics of synthetic ^{13}C-labeled melittin and three analogues in isotropic solvents have been studied by ^{13}C NMR and fluorescence techniques. While all of the

† This work was supported by Grant NI486K0521 from the Office of Naval Research. The NT-300 NMR spectrometer at IUPUI was purchased with partial support from The National Science Foundation (PCM 8018725). Purdue University Biochemical Magnetic Resonance Laboratory is supported by National Institutes of Health (RR01077). $K^{13}CN$ used in the synthesis of [^{13}C]Trp was provided in part by the Los Alamos Stable Isotope Resource, which is supported by the National Institutes of Health (RR02231) and the U.S. Department of Energy/Office of Health and Environmental Research Stable Isotope Program.

* Address correspondence to these authors.

‡ Mayo Foundation.

§ Indiana University–Purdue University at Indianapolis (IUPUI).

0006-2960/89/0428-8624$01.50/0

analogues retain the cytolytic activity of the native sequence, only melittin itself forms a soluble protein-like tetramer in aqueous media (Weaver et al., 1989). At least for melittin itself, it was reasoned that the Trp residue, which is freely accessible to solvent in the monomer, but partially buried in the tetramer (Terwilliger & Eisenberg, 1982a,b), would display a different rate and amplitude of indole side-chain motion in the two forms. Moreover, the random coil to helix transition that occurs upon tetramer formation or in the presence of methanol makes these peptides attractive models for the study of peptide chain mobility as well.

The "model-free" approach of Lipari and Szabo (1982a,b) has proved useful in extracting motional parameters from ^{13}C NMR relaxation data in several macromolecular systems (Hughes et al., 1984; Henry et al., 1986; Schmidt et al., 1987; Weaver et al., 1988; McCain et al., 1988). In the present work, this methodology was adopted for studies of ^{13}C-labeled synthetic melittin and analogues in water as a function of ionic strength, in water/methanol mixtures, and in dimethyl sulfoxide/water solutions. The mobility of the single ^{13}C-labeled Trp side chain at position 19, 17, 11 or 9 in the sequence of MLT-W19,[1] MLT-W17, MLT-W11, and MLT-W9, respectively, was monitored by measurement of the NMR relaxation parameters T_1^{-1} (spin–lattice relaxation rate), T_2^{-1} (spin–spin relaxation rate), and steady-state NOE (nuclear Overhauser effect). These quantities are sensitive to the motion of the $^{13}C\delta_1$–H bond vector, which is coplanar with the indole ring. Measurements of the steady-state fluorescence anisotropy and lifetime were used to follow the motion of the fluorescence emission dipole which also moves in concert with the indole moiety. In addition, [$^{13}C\alpha$]glycine was incorporated at position 12 in all of the peptides to provide a consistent marker for quantitation of peptide backbone motion by NMR alone.

The results of the present study are very encouraging from both a descriptive and quantitative viewpoint. It is shown that local motion of the Trp side chain does occur on a picosecond time scale and that the faster motions are generally of more restricted amplitude. Moreover, side-chain and peptide backbone motion are found to be quite sensitive to the solvent environment, conformation, and aggregation state of the peptide. The dynamics of the analogues are found to be consistent with structural features inferred from spectroscopic studies (Weaver et al., 1989). The model-free approach applied to analysis of combined fluorescence and NMR data yields values for rotational correlation times of the random coil or α-helical peptides that closely agree with values predicted on the basis of solvent-accessible surface area. In general, the model-free analysis of combined fluorescence and NMR data appears to be an excellent method for determining the amplitude and time scale of fluorophore mobility in peptides and proteins while also providing accurate overall correlation times.

Materials and Methods

Amino acid sequences and peptide synthetic methods are given in the preceding article (Weaver et al., 1989). Details of the cytolytic assay, gel filtration methods, and spectral characterization of the synthetic peptides are also described therein.

Steady-state fluorescence anisotropy values were measured on an SLM 4800 fluorometer with excitation at 295 nm (1-nm excitation band-pass), a vertically polarized excitation beam, and a cut-on filter (Schott WG 345) in the emission path. Fluorescence lifetimes were determined by multifrequency phase fluorometry (Gratton & Limkeman, 1983). The instrument used employs a mode-locked and frequency-doubled output from a Spectra-Physics 3000 Nd:YAG laser to synchronously pump a rhodamine 6-G dye laser. Output from the dye laser was cavity-dumped and then frequency-doubled to yield ultraviolet excitation tunable from ~285 to 320 nm. The multifrequency measurement exploits the harmonic content of the mode-locked laser as originally described by Gratton and Lopez-Delgado (1980). All fluorescence measurements were carried out at a peptide concentration of 20 μM in 10 mM Tris, pH 7.5, at 20 (±1) °C.

^{13}C NMR samples were prepared as described in the preceding article (Weaver et al., 1989). T_1, T_2, and steady-state NOE measurements were performed at 75.4 MHz on a Nicolet NT-300 FT spectrometer and at 50.3 MHz on a Varian XL-200 FT spectrometer. Relaxation measurements at 75.4 MHz used 12-mm NMR tubes containing ~2.5 mL of sample solution. Measurements at 50.3 MHz were performed on the same samples transferred to 20-mm NMR tubes with a coaxial cylindrical insert containing the sample. Broad-band noise decoupling of protons was used for T_1, T_2, and NOE measurements at 75.4 MHz; WALTZ decoupling (Shaka et al., 1983) was used at 50.3 MHz. All T_1 determinations employed a 180°–τ–90° inversion–recovery pulse sequence with a delay set to $\geq 5T_1$. Measurements of the spin–spin relaxation time were carried out by using a Carr–Purcell–Meiboom–Gill pulse sequence (Meiboom & Gill, 1958) with a composite 180° refocusing pulse to correct for field inhomogeneity and off-resonance fall off of field strength. T_1 and T_2 were extracted from the data by using either two- or three-parameter exponential fits. Gated decoupling was used to measure the NOE, alternate scans (with and without NOE) being collected into adjacent memory blocks. A delay of $\geq 9T_1$ was used between observation pulses in the NOE experiments due to the nonexponential decay of this relaxation parameter. At 75.4 MHz, relaxation data were typically collected as 8K data points with a spectral width of ±4505 Hz by using quadrature phase detection. At 50.3 MHz, relaxation data were collected as 6K data points with a spectral width of ±7758 Hz. All samples were maintained at a probe temperature of 20 (±1) °C.

Analysis of Fluorescence Data. If, in the decay of protein fluorescence anisotropy, $r(t)$, to zero as $t \rightarrow \infty$, the overall correlation time of the macromolecule (τ_m) is independent of the effective correlation time for hindered local or segmental motion of the fluorophore (τ_e), then the following empirical expression for the time-dependent anisotropy can be written:

$$r(t) = [(r_0 - r_\infty)e^{-t/\tau_e} + r_\infty]e^{-t/\tau_m} \quad (1)$$

The term r_0 is the fundamental anisotropy of the fluorophore, which is a function of the relative orientation of the absorption and emission transition dipoles at a given excitation wavelength, and r_∞ is the limiting hindered anisotropy (Kawato et al., 1977; Kinosita et al., 1977; Jähnig, 1979; Lakowicz et al., 1979; Engel & Prendergast, 1981). Equation 1 is conceptually identical with an expression derived by Lipari and Szabo (1980) in a theoretical treatment of fluorescent probes attached to macromolecules. Heyn (1979) has pointed out that the quantities r_0 and r_∞ can be related to an orientational order parameter S given by[2]

[1] Abbreviations: Bis-Tris, [bis(2-hydroxyethyl)amino]tris(hydroxymethyl)methane; CSA, chemical shift anisotropy; DMSO, dimethyl sulfoxide; ECEPP, empirical conformational energy program for peptides; MLT-W19, [[$^{13}C\delta_1$]-L-Trp-19,[$^{13}C\alpha$]Gly-12]melittin; MLT-W17, [[$^{13}C\delta_1$]-L-Trp-17,[$^{13}C\alpha$]Gly-12,Leu-19]melittin; MLT-W11, [[$^{13}C\delta_1$]-L-Trp-11,[$^{13}C\alpha$]Gly-12,Leu-19]melittin; MLT-W9, [[$^{13}C\delta_1$]-L-Trp-9,[$^{13}C\alpha$]Gly-12,Leu-19]melittin; MODLFREE, program based on a "model-free" approach to analysis and interpretation of NMR relaxation data; NOE, nuclear Overhauser effect.

$$S = (r_\infty/r_0)^{1/2} \quad (2)$$

Thus, the ratio r_∞/r_0 should describe the orientational order or spatial restriction imposed upon local or segmental motion of the fluorophore by the surrounding protein matrix.

The steady-state fluorescence anisotropy ($\bar{r}$) is much more convenient to measure than is $r(t)$. Under a given set of assumptions, steady-state data can be related to the orientational order parameter for rapid internal motion of a fluorophore. The steady-state anisotropy is given by

$$\bar{r} = \int_0^\infty r(t)\, F(t)\, dt / \int_0^\infty F(t)\, dt \quad (3)$$

where $F(t)$ is the time-dependent fluorescence intensity. If $F(t)$ is assumed to obey a single exponential decay law such that

$$F(t) = e^{-t/\tau_f} \quad (4)$$

where τ_f is the fluorescence lifetime, then substituting eq 1 and 4 into eq 3 gives

$$\bar{r} = \frac{(r_0 - r_\infty)}{1 + \tau_f(\tau_e^{-1} + \tau_m^{-1})} + \frac{r_\infty}{1 + (\tau_f/\tau_m)} \quad (5)$$

The Perrin relation (Perrin, 1934, 1936), characterizing the motion of simple fluorophores in isotropic environments, emerges from this expression as a limiting case where local motion is not considered (i.e., $\tau_e^{-1} \rightarrow 0$).

From eq 2 and 5, a mathematically allowed set of S and τ_e values can be derived from fluorescence lifetime and steady-state anisotropy data alone by the relation

$$\bar{r}/r_0 = \frac{(1 - S^2)}{1 + \tau_f(\tau_e^{-1} + \tau_m^{-1})} + \frac{S^2}{1 + (\tau_f/\tau_m)} \quad (6)$$

provided that one has a reliable value for the overall correlation time of the macromolecule in addition to a reasonably accurate r_0 value at the appropriate excitation wavelength. Equation 6 is the basis for analysis of Trp side-chain dynamics from fluorescence lifetime and steady-state anisotropy measurements on the synthetic peptides studied in this work.

Analysis of NMR Data. Information about motion of ^{13}C nuclei is contained in the relaxation rates T_1^{-1} and T_2^{-1} as well as the NOE. If the magnetic dipole–dipole interaction of the ^{13}C nucleus with its directly bonded proton or protons and chemical shift anisotropy (CSA) are taken to dominate these quantities, they can be written

$$T_1^{-1} = \frac{n\hbar^2\gamma_C^2\gamma_H^2}{4r_{CH}^6}[J(\omega_H - \omega_C) + 3J(\omega_C) + 6J(\omega_H + \omega_C)] + (\Delta\delta)^2\omega_C^2 J(\omega_C) \quad (7)$$

$$T_2^{-1} = \frac{n\hbar^2\gamma_C^2\gamma_H^2}{8r_{CH}^6}[4J(0) + J(\omega_H - \omega_C) + 3J(\omega_C) + 6J(\omega_H + \omega_C) + 6J(\omega_H)] + (1/6)(\Delta\delta)^2\omega_C^2 J(\omega_C)[4J(0) + 3J(\omega_C)] \quad (8)$$

$$\mathrm{NOE} = 1 + (\gamma_H/\gamma_C)[[6J(\omega_H + \omega_C) - J(\omega_H - \omega_C)]/[J(\omega_H - \omega_C) + 3J(\omega_C) + 6J(\omega_C + \omega_H) + (4r_{CH}^6/n\hbar^2\gamma_C^2\gamma_H^2)(\Delta\delta)^2\omega_C^2 J(\omega_C)]] \quad (9)$$

In these expressions, n is the number of protons directly bonded to the ^{13}C nucleus, $\hbar$ is Planck's constant divided by 2π, γ_C and γ_H are the magnetogyric ratios of ^{13}C and ^1H, respectively, r_{CH} is the carbon–proton distance, ω_C and ω_H are the ^{13}C and ^1H resonance frequencies, and $J(\omega)$ is the spectral density. The chemical shift tensor δ is assumed to be axially symmetric about the $^{13}C\delta_1$–H bond vector such that $\Delta\delta = \delta_\parallel - \delta_\perp$. CSA is assumed to be negligible for the Gly-12 α-carbon. Other potential contributions to relaxation of the indole ring $^{13}C\delta_1$ label that were considered, yet not included, were magnetic dipolar and scalar coupling with the pyrrole ^{14}N nucleus and magnetic dipolar interactions with nearby nonbonded protons. The first two interactions were determined to be negligible on the basis of the relatively small ^{14}N magnetogyric ratio and estimates of ^{14}N quadrupolar relaxation times. Although a dipolar contribution from nonbonded protons cannot be completely ruled out, examination of the crystal structure of tetrameric melittin did not reveal any nonbonded protons closer than ~2.5 Å to $C\delta_1$. Such protons would contribute negligibly to dipolar relaxation in comparison with a directly bonded proton.

The spectral density proposed by Lipari and Szabo (1982a,b)

$$J(\omega) = \frac{2}{5}\left[\frac{\mathcal{S}^2\tau_m}{1 + \omega^2\tau_m^2} + \frac{(1 - \mathcal{S}^2)\tau}{1 + \omega^2\tau^2}\right] \quad (10)$$

where $\tau^{-1} = \tau_e^{-1} + \tau_m^{-1}$ is used in the preceding expressions for T_1, T_2, and NOE. In this expression, $\mathcal{S}$ is a "generalized" order parameter for local motion of a given ^{13}C–H vector and τ_e and τ_m are as defined previously. The spectral density is derived from an expression for the autocorrelation function of the ^{13}C–H vector assuming that overall molecular motion is isotropic and that internal and overall motions are independent. For the ^{13}C-labeled peptides of this study, the appropriate vector is either the Trp $^{13}C\delta_1$–H bond vector or, for $^{13}C\alpha$-labeled Gly-12, a mean vector lying in the plane defined by the two Cα–H bonds. Provided that the indole ring is rigid and planar, the motion of the $^{13}C\delta_1$–H vector should reflect that of the Trp side chain as a whole. For glycine, the motion of the mean $^{13}C\alpha$–H_2 bond vector should be indicative of the flexibility of the peptide chain in the vicinity of the labeled residue.

Given a set of T_1, T_2, and NOE data, the motional variables $\mathcal{S}$, τ_e, and τ_m can be derived by evaluating the nonlinear system defined by eq 7–10. A unique solution, if it exists, requires the measurement of three independent relaxation values, i.e., T_1, T_2, and NOE at a single spectrometer frequency or other combinations at more than one frequency. When fewer than three relaxation values are known, constraints on $\mathcal{S}$, τ_e, and τ_m can be established from the available data. A computer program (MODLFREE) was developed that finds allowed values for $\mathcal{S}$, τ_e, and τ_m given any number of experimental relaxation measurements obtained at one or more spectrometer frequencies. The program employs a simple grid-search algorithm using parabolic interpolation to find local and absolute minima on the χ^2 hypersurface pertaining to the system of nonlinear equations (Bevington, 1969). All calculations were done by using MODLFREE implemented on an IBM PC AT compatible computer.[3]

If MODLFREE is provided with only a single relaxation measurement, the algorithm requires specification of a fixed

[2] The order parameter derived experimentally from fluorescence measurements is denoted by an italicized S, and the experimentally derived NMR order parameter by a script $\mathcal{S}$. When both fluorescence and NMR data are used in combined analyses, the composite experimentally derived order parameter is denoted by a nonitalicized, nonscript S.

[3] A compiled version of this program is available from one of us (A.J.W.) upon request.

τ_m; all $\mathcal{S}$ and τ_e values consistent with the single observable and this τ_m are then calculated. If two relaxation measurements are available, the spectral density is systematically evaluated over all τ_m values specified as "physically reasonable"; $\mathcal{S}$ and τ_e are adjusted at each τ_m until the calculated and observed relaxation values agree. In this situation, the results can then be presented in the form of plots of $\mathcal{S}$ or τ_e as a function of τ_m. Such plots are often referred to below as T_1–NOE curves since they are generated from such data obtained at a single spectrometer frequency. If three or more relaxation values are available, a "unique" solution to the system of equations is sought which represents a least-squares fit of the calculated to the observed relaxation values. The statistic measuring goodness of fit is computed as

$$\chi^2 = \sum_{\omega}\left[\frac{(T_1^{obs} - T_1^{calc})^2}{(T_1^{obs})^2} + \frac{(T_2^{obs} - T_2^{calc})^2}{(T_2^{obs})^2} + \frac{(NOE^{obs} - NOE^{calc})^2}{(NOE^{obs})^2}\right] \quad (11)$$

where the sum is taken over measurements at one or more spectrometer frequencies. In general, T_1–NOE curves were found to be the better method for interpreting the derived motional parameters since exact ($\chi^2 = 0$) fits of single-frequency T_1, T_2, and NOE data do not readily allow one to assess the probable error. T_1–NOE curves, on the other hand, provide a ready visual appreciation of the potential variation in $\mathcal{S}$ and τ_e as a function of τ_m as well as an ascertainment of the uncertainty in motional parameters corresponding to a given pair of measured relaxation values.

The behavior of the T_1, T_2, and NOE expressions with respect to $\mathcal{S}$, τ_e, τ_m is not easily discerned by simple inspection of eq 7–10. It is therefore instructive to simulate experimental results by explicitly plotting the observables as functions of the motional parameters. In panels a of Figures 1–3, T_1, T_2, and NOE are each shown as a function of the overall correlation time at selected values for $\mathcal{S}$ and τ_e. When $\mathcal{S} = 1$, the relaxation parameters are the characteristic monotonic functions of a single correlation time (τ_m). However, as the order parameter decreases, the contribution of a faster local motion to the spectral density increases. For very small $\mathcal{S}$ values, the correlation time for the macromolecule influences the relaxation parameters only when $\tau_m \cong \tau_e$. However, in the more usual situation where $\tau_m > \tau_e$, T_1, T_2, and NOE are relatively insensitive to τ_m when $\mathcal{S}$ is small.

Lipari and Szabo (1982b) give a set of empirical rules by which the accuracy of experimentally determined motional parameters can be assessed. The restrictions defined by those rules are shown as shaded regions in panels b of Figures 1–3, in which the amplitude ($\mathcal{S}$) of the internal motion is plotted as a function of its rate (τ_e) for a wide range of T_1, T_2 and NOE values. According to the empirical rules, experimentally derived motional parameter values lying within the shaded area should be suspect. It is apparent that the rules generally require that regions of rapid variation of $\mathcal{S}$ with τ_e be avoided. Examination of the curves themselves, in lieu of the empirical rules, should provide for a more accurate assessment of the potential error in motional parameter values determined by experiment.

Analysis of Combined Fluorescence and NMR Data. Equation 6 posits a relationship of the steady-state fluorescence anisotropy and fluorescence lifetime to the model-free motional parameters contained in the NMR spectral density (eq 10). Indeed, Lipari and Szabo (1980) have pointed out the formal

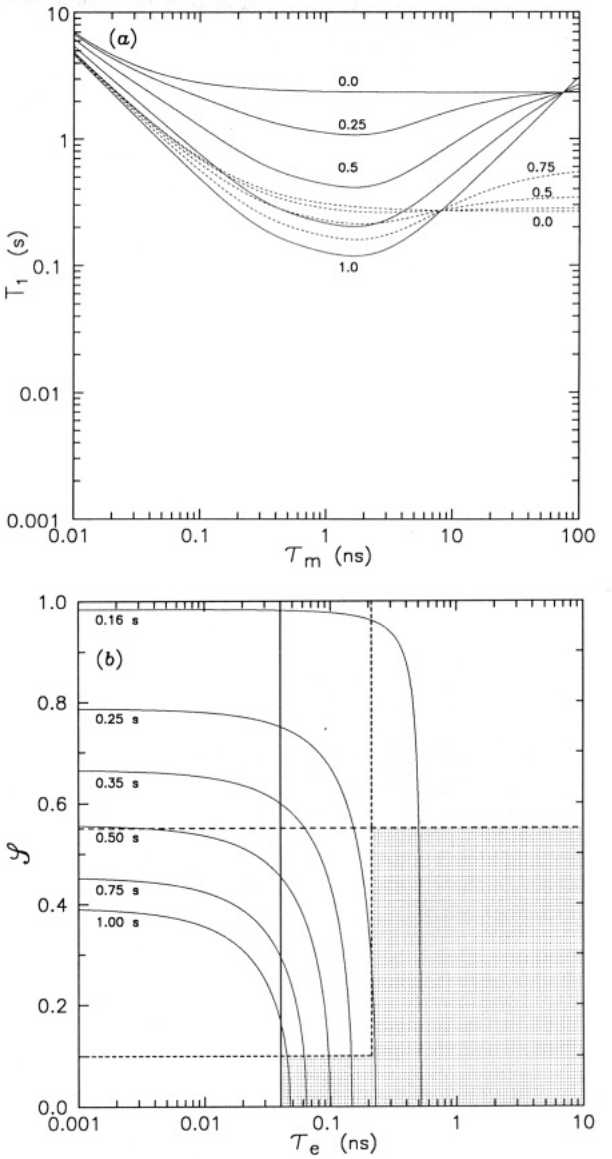

FIGURE 1: In panel a, the spin–lattice relaxation time, T_1, is plotted as a function of the overall correlation time, τ_m, for order parameter ($\mathcal{S}$) values of 0.0, 0.25, 0.5, 0.75, and 1.0, at effective correlation time (τ_e) values of 0.02 ns (—) and 0.2 ns (---). For clarity, some curves are not labeled with order parameter values. In panel b, $\mathcal{S}$ is plotted as a function of τ_e for T_1 values of 0.16, 0.25, 0.35, 0.50, 0.75, and 1.00 s, at τ_m = 4 ns. Shaded areas indicate regions of potentially unreliable experimental motional parameter values as defined by a set of empirical rules given by Lipari and Szabo (1982b). Experimental motional parameter values falling within *unshaded* regions delimited by the appropriate vertical and/or horizontal lines are accurate to within (i) "a few percent" when $\tau_e/\tau_m \leq 0.01$ *and* $(\omega_C + \omega_H)\tau_e \leq 0.1$ (—); (ii) ~25% when $\tau_e/\tau_m \leq 0.5$ *and* $\mathcal{S} \geq 0.1$ *and* $(\omega_C + \omega_H)\tau_e \leq 0.5$ (--); and (iii) ~15% when $\mathcal{S} \geq 0.55$ (---). In (a) and (b), n = 1, r_{CH} = 1.09 Å, $\Delta\delta$ = 0 ppm, $\omega_C = 2\pi(75.4)$ MHz, and $\omega_H = 2\pi(300.1)$ MHz.

similarity between fluorescence depolarization and NMR relaxation theory which underlies the derivation of the fluorescence and NMR equations used here. Under certain constraints, these expressions provide a common formalism which may yield an improved description of fluorophore dynamics based on the use of combined fluorescence and NMR data. If this approach is to be taken, the validity of certain assumptions is essential: (a) colinearity of the $^{13}C\delta_1$–H bond and the fluorescence dipole vectors; (b) motion of these vectors in a concerted fashion with the planar indole ring; and (c) the ability of the model-free approach to adequately describe Trp side-chain dynamics in terms of two motional parameters,

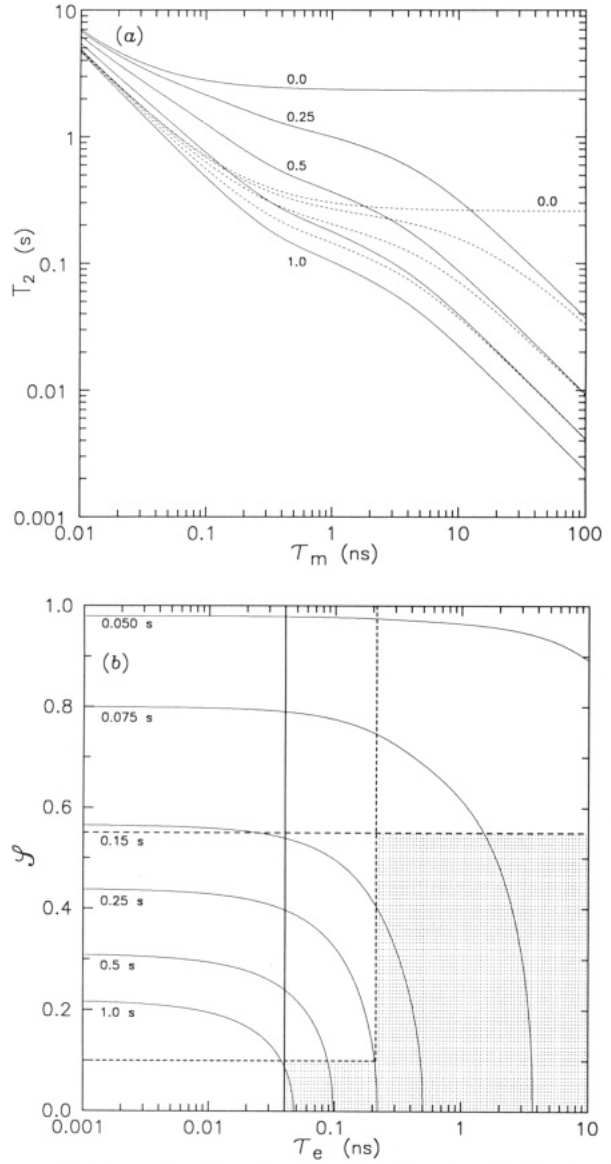

FIGURE 2: In panel a, the spin–spin relaxation time, T_2, is plotted as a function of the overall correlation time, τ_m, for order parameter ($\mathcal{S}$) values of 0.0, 0.25, 0.5, 0.75, and 1.0, at effective correlation time (τ_e) values of 0.02 ns (—) and 0.2 ns (---). For clarity, some curves are not labeled with order parameter values. In panel b, $\mathcal{S}$ is plotted as a function of τ_e for T_2 values of 0.05, 0.075, 0.15, 0.25, 0.5, and 1.0 s, at τ_m = 4 ns. Shaded areas indicate regions of potentially unreliable experimental motional parameter values (see Figure 1 caption for details). In (a) and (b), n = 1, r_{CH} = 1.09 Å, $\Delta\delta$ = 0 ppm, ω_C = 2π(75.4) MHz, and ω_H = 2π(300.1) MHz.

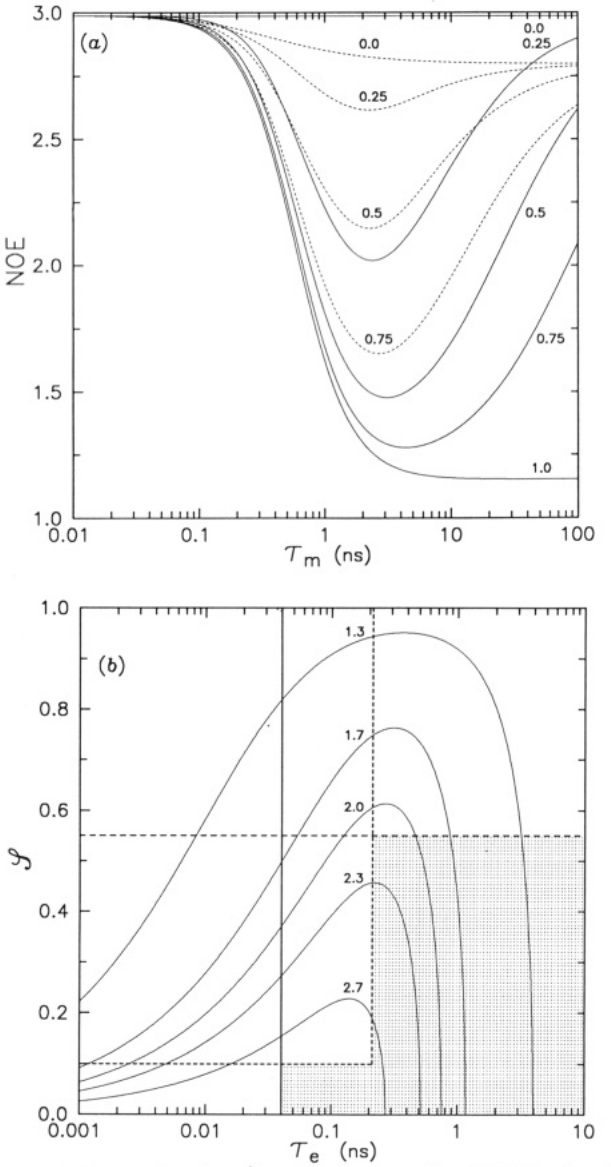

FIGURE 3: In panel a, the nuclear Overhauser effect, NOE, is plotted as a function of the overall correlation time, τ_m, for order parameter ($\mathcal{S}$) values of 0.0, 0.25, 0.5, 0.75, and 1.0, at effective correlation time (τ_e) values of 0.02 ns (—) and 0.2 ns (---). In panel b, $\mathcal{S}$ is plotted as a function of τ_e for NOE values of 1.3, 1.7, 2.0, 2.3, and 2.7, at τ_m = 4 ns. Shaded areas indicate regions of potentially unreliable experimental motional parameter values (see Figure 1 caption for details). In (a) and (b), n = 1, r_{CH} = 1.09 Å, $\Delta\delta$ = 0 ppm, ω_C = 2π(75.4) MHz, and ω_H = 2π(300.1) MHz.

namely $\mathcal{S}$ and τ_e.

Given the verity of these assumptions, implementation of the combined analysis is straightforward since eq 6 can be treated by MODLFREE in the same manner as the NMR expressions (eq 7–10). The fluorescence observables were measured at an excitation wavelength of 295 nm. With red edge excitation, the fluorescence dipoles and the $^{13}C\delta_1$–H bond vector are approximately colinear (Lakowicz et al., 1983). In analyses of combined fluorescence and NMR data presented below, the measured steady-state fluorescence anisotropy and fluorescence lifetime are substituted for the NMR spin–spin relaxation time since the latter was usually the least accurate of the NMR observables. This approach yields motional parameter values that agree closely with the those determined from NMR data alone and thus appears to be of potential use in augmenting the model-free description of side-chain dynamics.

RESULTS

The quantitative interpretation of $\mathcal{S}$ and τ_e values was found to depend critically on having an accurate value for the overall correlation time of the macromolecule. Thus, rotational correlation times were calculated for the various structural forms of melittin in the appropriate isotropic solvents. Agreement between predicted and experimental τ_m values was deemed a prerequisite for valid interpretation of least-squares $\mathcal{S}$ and τ_e values describing local motion. In cases where predicted and observed τ_m values did not agree well, meaningful values for $\mathcal{S}$ and τ_e could still be extracted from T_1–NOE curves on the basis of the predicted overall correlation times.

Interpretation of Overall Rotational Correlation Times. In general, the accuracy of protein rotational correlation times determined by fluorescence depolarization or NMR has been difficult to assess due to the fact that observed τ_m values for

small globular proteins are typically 1.5–2.5 times greater than values calculated from the Stokes–Einstein–Debye relation[4] even when protein shape and hydration are considered [e.g., see Bauer et al. (1975) and Massey and Churchich (1979)]. An empirical method based on calculation of the solvent-accessible protein surface area is introduced here which intrinsically accounts for protein shape and hydration and which diminishes the usual discrepancy between experimental and predicted overall correlation time values. Rotational correlation times based on solvent-accessible surface area are compared below with theoretical values determined by other methods for (1) unstructured (random coil) melittin monomer, (2) α-helical melittin monomer, and (3) melittin tetramer.

(1) Unstructured Melittin Monomer. For the unstructured peptide monomers in water, overall rotational correlation times of 4.1 and 6.0 ns were calculated from the Stokes–Einstein–Debye relation assuming that the peptides behave as "random coil" poly(L-alanine) chains 26 residues in length[5] (Brant & Flory, 1965a,b). The lower correlation time value was derived for such a peptide containing two randomly placed glycine residues[6] (Miller et al., 1967), while the larger value obtains for a 26-mer without glycyl residues. With the exception of Gly and Pro residues, the amino acid composition of a given random coil peptide should not greatly affect its overall correlation time; steric constraints introduced by groups beyond the β-carbon of peptide side chains appear to have little effect on the conformational space allowed to an unstructured peptide chain (Brant & Flory, 1965a). It should therefore be reasonable to model unstructured melittin and analogues in this fashion.

In this work, an alternative empirical method of calculating expected τ_m values from the solvent-accessible protein surface area was adopted. This was thought to be a reasonable approach since stick boundary conditions relate frictional drag to the solvent-accessible surface area of a macromolecule. By use of a probe sphere of 1.4-Å radius, the solvent-accessible surface area of the extended, fully solvent-exposed melittin chain was computed according to an algorithm developed by M. L. Connolly (unpublished results, 1986). Atomic coordinates for the extended peptide, inclusive of protons, were generated by using CHARMM (Brooks et al., 1983). van der Waals radii used in all calculations of solvent-accessible surface area were values derived from ECEPP parameters for 6–12 nonbonded potentials for pairs of like atoms (Némethy et al., 1983). The protein surface area inclusive of hydrogen atoms (A = 2434 Å^2) was then used to calculate the radius of an equivalent sphere as $r = (A/4\pi)^{1/2}$. Hydration was included by adding 2.8 Å (the thickness of a single water layer) to the equivalent sphere radius. By this method, effective hydrodynamic volumes of 1.13×10^{-20} and 1.96×10^{-20} cm^3 were determined for the nonhydrated and hydrated extended melittin chains, respectively. Using the Stokes–Einstein–Debye relation, one then finds overall rotational correlation times in water of 2.8 and 4.8 ns. The latter agrees with values determined above from statistical chain dynamics calculations.

Table I: Steady-State Fluorescence Anisotropy Values, Mean Fluorescence Lifetimes, Estimated Overall Correlation Times, and Plateau Values for the Trp Side-Chain Order Parameter and Effective Correlation Time for MLT-W19 and Analogues in Water or 2 M NaCl[a]

	$\bar{r}$	τ_f (ns)	τ_m (ns)	$S_{max} \rightarrow S_{0.9}$	$\tau_{e,0.9}$ (ns)
			MLT-W19		
H_2O	0.039	2.75	4.8	0.59 → 0.53	0.19
2 M NaCl	0.100	2.17	13.7	0.82 → 0.74	0.63
			MLT-W17		
H_2O	0.038	2.56	4.8	0.57 → 0.51	0.18
			MLT-W11		
H_2O	0.041	2.12	4.8	0.58 → 0.52	0.15
			MLT-W9		
H_2O	0.044	2.47	4.8	0.62 → 0.56	0.18

[a] $S_{max} \rightarrow S_{0.9}$ and $\tau_{e,0.9}$ are derived from plots of $S(\tau_e)$ on the basis of eq 6 (cf. Figure 4). Steady-state anisotropy values were measured by using an excitation wavelength of 295 nm, at which r_0 = 0.175 for monomeric melittin (Lakowicz et al., 1983). All fluorescence measurements were carried out at a peptide concentration of 20 μM in 10 mM Tris, pH 7.5, at 20 (±1) °C.

When corrected to the viscosity of 90% DMSO/D_2O (η = 2.12 cP), in which NMR relaxation data were also collected, the corresponding τ_m values become 5.9 and 10.2 ns.

(2) α-Helical Melittin Monomer. Theoretical estimates of the overall correlation time depend on the particular structural model and the assumed molecular dimensions of α-helical melittin monomer. When the monomer is modeled as a prolate ellipsoid with an axial ratio between 3.0 and 4.0 (from crystallographic dimensions), one finds overall correlation times of 1.8–2.0 ns based on the molecular weight, partial specific volume, and estimated hydration of α-helical melittin monomer.[7] However, correlation times determined from the solvent-accessible surface area of the melittin α-helix (A = 1984 Å^2) are substantially greater. Proton positions were calculated from the crystallographic coordinates for C, N, and O atoms of the A chain of melittin tetramer (Terwilliger & Eisenberg, 1982a,b). Using ECEPP van der Waals radii, one finds effective hydrodynamic volumes of 8.31×10^{-21} and 1.52×10^{-20} cm^3 for nonhydrated and hydrated α-helical melittin, which correspond to overall correlation times in water of 2.1 and 3.8 ns, respectively, for the equivalent spheres. When corrected for shape,[7] the predicted τ_m values are 3.0 and 5.5 ns.

(3) Melittin Tetramer. Recent time-resolved fluorescence and ESR measurements on melittin tetramer have generated overall correlation times for this protein ranging from 3.4 ns (Lakowicz et al., 1987) to 5.6 ns (John & Jähnig, 1988) to ~20 ns (Altenbach & Hubbell, 1988). The sources of dis-

[4] $\tau_m = V_h\eta/kT$, where V_h is the hydrated molecular volume, η is the bulk viscosity of the medium, k is Boltzmann's constant, and T is the absolute temperature.

[5] In this case, $\tau_m = 4\pi\langle r_g^2\rangle^{3/2}\eta/(3kT)$, where $\langle r_g^2\rangle$ is the mean-square radius of gyration of the polymer chain.

[6] Glycine residues are found at positions 1, 3, and 12 in melittin and each of the synthetic peptides. A proline residue is located at position 14 of each sequence. It was assumed that the increased flexibility imparted by one of the Gly residues would be negated by the single proline residue; thus, two Gly residues were used in calculating the expected range of τ_m values for the random coil peptides.

[7] The volume, V_h, occupied by a hydrated particle was calculated as $V_h = f(M/N)(\bar{V}_2 + \delta_1\bar{V}_1)$, where M is the molecular weight, N is Avogadro's number, $\bar{V}_2$ is the partial specific volume of the nonhydrated protein, $\bar{V}_1$ is the partial specific volume of the solvent, δ_1 gives the hydration of the particle, and f is a particle shape factor. In calculations for melittin monomer and tetramer, respectively, M = 2848 and 11 392 daltons, η = 0.01 P, T = 293 K, $\bar{V}_2$ = 0.71 cm^3 g^{-1} (Terwilliger & Eisenberg, 1982b), δ_1 = 0.4 g of H_2O (g of protein)$^{-1}$, which is a typical value for globular proteins, and $\bar{V}_1$ = 1.0 cm^3 g^{-1}. For prolate ellipsoids, a Perrin shape factor, $1 \le f \le 2$, can be related to the harmonic mean of rotational correlation times, τ_a and τ_b, of the major and minor axes of the ellipse, respectively, i.e., $\tau_m^{-1} = (1/3)[\tau_a^{-1} + 2(\tau_b^{-1})]$. The shape factor was defined as $f = 3F_aF_b/(2F_a + F_b)$, where $F_a = f_a/f_{sph}$ and $F_b = f_b/f_{sph}$ are the frictional coefficients for rotational motion about the major and minor axis, respectively, of a prolate ellipsoid relative to that of an equivalent volume sphere [cf. Cantor and Schimmel (1980)]. For prolate ellipsoids with axial ratios of 3–4 (α-helical melittin monomer), f = 1.37–1.52; for a prolate ellipsoid of axial ratio $^3/_2$ (melittin tetramer), f = 1.06.

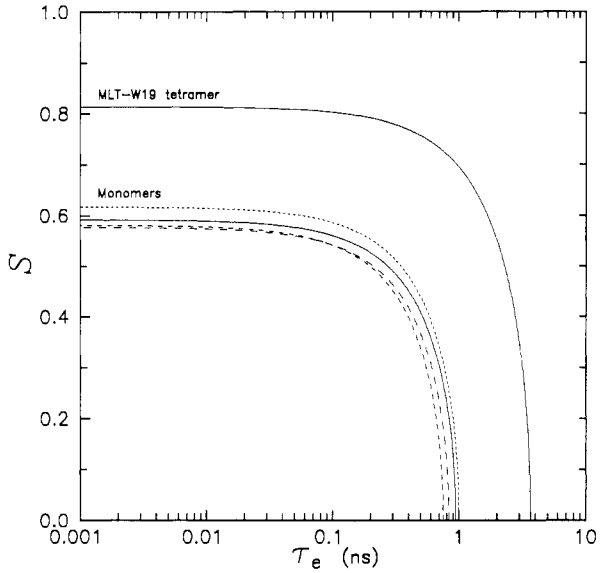

FIGURE 4: Fluorescence-derived order parameter (S) as a function of the effective correlation time (τ_e) for local motion of the Trp side chain of MLT-W19 and analogues in H_2O or 2 M NaCl. MLT-W19 (—); MLT-W17 (– –); MLT-W11 (- - -); MLT-W9 (···). These plots are based on eq 6, using $\bar{r}$ and τ_f data given in Table I. For the monomeric samples, a τ_m value of 4.8 ns was assumed. For MLT-W19 tetramer, a τ_m value of 13.7 ns was used.

parity between values extracted by the various techniques are not obvious.

Assuming that melittin tetramer can be adequately modeled as a hydrated prolate ellipsoid with an axial ratio of $^3/_2$ (Terwilliger & Eisenberg, 1982a), we calculate a value of 5.5 ns for its overall correlation time in water. In contrast, the correlation time of the tetramer as determined from its solvent-accessible surface area (A = 5221 Å^2) is approximately 2-fold larger. Proton positions were calculated from the crystallographic coordinates for C, N, and O atoms of melittin tetramer (Terwilliger & Eisenberg, 1982a,b). Using ECEPP van der Waals radii, one finds effective hydrodynamic volumes of 3.55×10^{-20} and 5.22×10^{-20} cm^3 for nonhydrated and hydrated melittin tetramer, which correspond to overall correlation times of 8.8 and 12.9 ns, respectively, for the equivalent spheres. When corrected for shape,[7] the predicted τ_m values are 9.3 and 13.7 ns.

Fluorescence Studies. Steady-state anisotropy values and mean fluorescence lifetimes for the peptides in water or in the presence of 2 M NaCl are compiled in Table I. Melittin fluorescence lifetimes have been found to exhibit single-exponential or multiexponential decays depending on the excitation and emission wavelengths and sample conditions (Georghiou et al., 1982; Tran & Beddard, 1985; Lakowicz et al., 1983, 1986). However, values for the mean unquenched fluorescence lifetime measured previously appear to be in good agreement with one another and with τ_f values measured for MLT-W19 under similar experimental conditions. In particular, the decrease in τ_f observed for MLT-W19 with increasing NaCl concentration has been noted previously for the naturally occurring peptide (Lakowicz et al., 1983).

From steady-state fluorescence anisotropy and fluorescence lifetime data alone, S and τ_e cannot be determined independently. However, such data can be used to generate S as a function of τ_e from eq 6 for the Trp side chain provided that an estimate for τ_m is available. $S(\tau_e)$ curves are drawn in Figure 4 for MLT-W19 and analogues in water and for MLT-W19 tetramer in 2 M NaCl. Experimental τ_f and $\bar{r}$ values in conjunction with the predicted τ_m of 4.8 ns for the hydrated random coil monomer (see above) result in very similar $S(\tau_e)$ curves for MLT-W19 and the analogues. $S(\tau_e)$ is also plotted for MLT-W19 tetramer assuming the appropriate τ_m value to be that of hydrated melittin tetramer (13.7 ns).

From the near equivalence of the curves generated for the monomeric peptides in water, one can conclude that order parameters for MLT-W19 and analogues are likely to be similar if τ_e values for the respective Trp side chains are also similar. The plateau region of these curves corresponds to $\tau_e \ll \tau_f$, which is certainly valid if fluorophore motion occurs on a subnanosecond time scale. Figure 4 shows that the order parameter is relatively insensitive to τ_e in the plateau region. Thus, although a large range of τ_e values is allowed by the fluorescence data, the choice of S is limited. Still, it is useful to know the largest τ_e value below which the order parameter is effectively constant valued (i.e., S still within the plateau region). The value of τ_e corresponding to $0.9S_{max}$ was arbitrarily chosen to represent this quantity and is designated $\tau_{e,0.9}$. The corresponding order parameter value is denoted by $S_{0.9}$. In Table I, $\tau_{e,0.9}$ values and $S_{max} \rightarrow S_{0.9}$ ranges are specified for each of the curves shown in Figure 4.

Plateau S values for local Trp side-chain motion in monomeric MLT-W19 and analogues in water fall between 0.52 and 0.62, assuming τ_m = 4.8 ns. If this estimate for τ_m is accurate, and the limit $\tau_e \ll \tau_f$ applies, then an approximate *upper* limit of $\tau_{e,0.9}$ = 0.15–0.19 ns can be placed on the effective correlation time for Trp side-chain motion from fluorescence data alone. Thus, under the assumptions of a reasonably accurate τ_m value and local fluorophore motion much faster than its radiative rate, values for S and τ_e become available for comparison with their NMR-derived counterparts.

Given the estimated τ_m value of 13.7 ns, Figure 4 predicts plateau S values of 0.74–0.82 for tetrameric MLT-W19 in water. Although the order parameter is clearly larger than in the monomeric peptides, it cannot be determined from analysis of the fluorescence data alone whether the effective correlation time for indole ring motion in the tetramer is shorter or longer than in the monomer. Fluorescence-derived S values for the peptide monomers and MLT-W19 tetramer are shown below to be in good agreement with NMR-derived values. Moreover, the NMR experiments provide additional motional information to yield a consistent description of fluorophore dynamics in these peptides.

NMR Studies. ^{13}C NMR relaxation data, compiled in Table II, were obtained at 75.4 MHz for MLT-W19 and analogues dissolved in buffered DMSO-d_6/D_2O, D_2O/CD_3OD, D_2O, and D_2O/NaCl solutions. Least-squares values for the model-free motional parameters derived from the data in Table II are given in Table III. Relaxation data and motional parameters (not shown) were also determined at 50.3 MHz for selected peptide samples. In general, results obtained at the lower spectrometer frequency were consistent with those determined at 75.4 MHz.

A few general comments are in order before discussing specific results. First, accurate measurement of short T_2 values $< \sim$30 ms was problematic since instrumental response time often represented a significant fraction of T_2. Because this factor was not accounted for in extracting relaxation times from the raw data, T_2 values are very likely overestimated. It should be noted that T_2 values were typically smaller, and hence more error prone, for the Gly-12 Cα than for the Trp Cδ_1. Second, chemical shift anisotropy was expected to be a significant relaxation mechanism for the ^{13}Cδ_1 label in the Trp

Table II: ^{13}C NMR Relaxation Data Obtained at 75.4 MHz for MLT-W19 and Analogues in Buffered DMSO-d_6/D_2O, D_2O/CD_3OD, D_2O, and D_2O/NaCl

		Trp Cδ_1			Gly-12 Cα		
solvent	sample [concn (mM)]	T_1 (s)[a]	T_2 (s)[b]	NOE[c]	T_1 (s)	T_2 (s)	NOE
DMSO-d_6/10% D_2O (v/v)	MLT-W19 (5.55)[d]	0.195	0.016	1.55	0.129	0.006	1.34
	MLT-W17 (5.83)	0.192	0.015	1.54	0.123	0.010	1.43
	MLT-W11 (5.35)	0.199	0.015	1.59	0.134	0.005	1.47
	MLT-W9 (6.13)	0.198	0.024	1.51	0.145	0.008	1.59
D_2O/10–30% CD_3OD (v/v)	MLT-W19 (1.00)[e]	0.222	0.025	1.69	0.101	0.018	1.85
	MLT-W19 (0.89)	0.150	0.031	1.49	0.095	0.008	1.45
	MLT-W19 (0.78)	0.194	0.028	1.59	0.099	0.011	1.30
	MLT-W17 (1.15)[f]	0.190		1.45	0.105		1.44
	MLT-W11 (1.29)	0.238	0.032	1.74	0.111	0.013	1.40
	MLT-W19 (4.57)[g]	0.238	0.020	1.39	0.205	0.010	1.41
	MLT-W19 (4.06)	0.273	0.020	1.30	0.207	0.009	1.31
	MLT-W19 (3.56)	0.280	0.014	1.45	0.201	0.007	1.43
D_2O	MLT-W19 (1.11)[h]	0.182	0.030	1.78	0.101	0.017	2.06
	MLT-W17 (0.86)	0.191	0.007	1.80	0.141	0.009	1.75
	MLT-W11 (1.29)	0.205	0.028	1.59	0.103	0.014	1.42
	MLT-W19 (5.08)[i]	0.267	0.018	1.32	0.173	0.014	1.16
	MLT-W19 (5.55)	0.273	0.020	1.25	0.157	0.013	1.32
	MLT-W19 (6.17)	0.274	0.015	1.25	0.173	0.012	1.37
D_2O/0.05–1.0 M NaCl	MLT-W19 (6.09)[j]	0.300	0.017	1.41	0.172	0.011	1.29
	MLT-W19 (5.86)	0.231	0.017	1.27	0.169	0.017	1.16
	MLT-W19 (5.40)	0.247	0.017	1.21	0.187	0.014	1.36
	MLT-W19 (4.62)	0.232	0.015	1.24	0.188	0.017	1.27
	MLT-W17 (1.01)[k]	0.232	0.021	1.28	0.145	0.015	1.63
	MLT-W17 (0.86)	0.191	0.007	1.80	0.141	0.009	1.75

[a] Experimental uncertainty in T_1 values was ±0.003–0.005 s. [b] Experimental uncertainty in T_2 values was ±0.001–0.003 s. [c] Experimental uncertainty in NOE values was ±0.03–0.05. [d] 50 mM Bis-Tris, pH 6.0. [e] 10 mM Bis-Tris, pH 6.0; samples contained 10%, 20%, and 30% CD_3OD, respectively. [f] 10 mM Bis-Tris, pH 6.0, 20 °C; samples contained 30% CD_3OD. T_2 values were not measured for this sample. [g] 50 mM Bis-Tris, pH 6.0; samples contained 10%, 20%, and 30% CD_3OD, respectively. [h] 10 mM Bis-Tris, pH 6.0. [i] 50 mM Bis-Tris, pH 6.0; relaxation data obtained for two of these samples (5.08 mM and 6.17 mM) provided base-line values for subsequent titration with CD_3OD and NaCl, respectively. [j] 50 mM Bis-Tris, pH 6.0; samples contained 0.05, 0.2, 0.5, and 1.0 M NaCl, respectively. [k] 10 mM Bis-Tris, pH 6.0; samples contained 0.5 and 1.0 M NaCl, respectively. All pH values are uncorrected meter readings. All measurements were carried out at a probe temperature of 20 °C.

Table III: Least-Squares Analysis of Relaxation Data Obtained at 75.4 MHz for MLT-W19 and Analogues in Buffered DMSO-d_6/D_2O, D_2O/CD_3OD, D_2O, and D_2O/NaCl[a]

		Trp Cδ_1			Gly-12 Cα		
solvent	sample [concn (mM)]	$\mathcal{S}$	τ_e (ns)	τ_m (ns)	$\mathcal{S}$	τ_e (ns)	τ_m (ns)
DMSO-d_6/10% D_2O (v/v)	MLT-W19 (5.55)	0.82	0.56	13.5	0.77	1.68	31.7
	MLT-W17 (5.83)	0.81	0.59	13.9	0.78	1.27	18.9
	MLT-W11 (5.35)	0.80	0.54	14.7	0.76	1.23	39.0
	MLT-W9 (6.13)	0.82	0.20	8.5	0.80	0.91	24.4
D_2O/10–30% CD_3OD (v/v)	MLT-W19 (1.00)	0.75	0.19	9.8	0.61	0.68	15.0
	MLT-W19 (0.89)	0.81	0.33	6.3	0.61	1.34	38.3
	MLT-W19 (0.78)	0.77	0.20	8.0	0.67	2.03	20.4
	MLT-W17 (1.15)[b]						
	MLT-W11 (1.29)	0.69	0.15	8.9	0.76	1.37	14.9
	MLT-W19 (4.57)	0.86	0.12	9.9	0.95	0.25	13.2
	MLT-W19 (4.06)	0.84	0.06	10.2	0.96	0.75	14.5
	MLT-W19 (3.56)	0.89	0.17	13.6	0.91	0.97	21.0
D_2O	MLT-W19 (1.11)	0.70	0.29	8.7	0.53	0.56	21.6
	MLT-W17 (1.15)	0.67	0.21	6.5	0.87	0.44	6.8
	MLT-W11 (1.29)	0.77	0.18	8.3	0.72	1.34	14.4
	MLT-W19 (5.08)	0.86	0.08	10.7	>0.99		10.0[c]
	MLT-W19 (5.55)	0.85	0.04	10.1	0.84	0.27	10.4
	MLT-W19 (6.17)	0.93	0.11	12.3	0.95	0.25	10.6
	MLT-W17 (5.74)	0.84	0.27	10.4	0.75	0.88	16.9
D_2O/0.05–1.0 M NaCl	MLT-W19 (6.09)	0.84	0.09	12.4	0.96	0.73	11.3
	MLT-W19 (5.86)	0.92	0.13	10.2	>0.99		9.7[d]
	MLT-W19 (5.40)	0.92	0.07	10.3	0.90	0.08	10.1
	MLT-W19 (4.62)	0.95	0.18	10.7	0.88	0.03	8.9
	MLT-W17 (1.01)	0.87	0.08	9.0	0.88	0.36	9.9
	MLT-W17 (0.86)	0.67	0.57	43.7	0.77	0.71	22.4

[a] Least-squares results correspond to data collected in Table II. In least-squares analyses of [$^{13}C\delta_1$]Trp data, $n = 1$, $r_{CH} = 1.09$ Å, and $\Delta\delta = 200$ ppm; for [$^{13}C\alpha$]Gly, $n = 2$, $r_{CH} = 1.10$ Å, and $\Delta\delta = 0$ ppm. χ^2 values were zero (i.e., exact fits of the observed to calculated values) unless otherwise noted. The estimated error in motional parameter values is ±15% (cf. Figure 1 caption). [b] Least-squares analysis was not possible since T_2 values were not measured for this sample. [c] $\chi^2 = 0.0004$. [d] $\chi^2 = 0.0014$.

side chain—a maximal contribution of CSA to its relaxation was estimated to be $\Delta\delta = 200$ ppm (Veeman, 1984; Parhami & Fung, 1985), inclusion of which was found to substantially reduce the magnitude of the χ^2 error function (eq 11) in

least-squares fits. In general, Trp side-chain order parameters were increased by ~5%, and τ_e and τ_m were lowered by 10–50% when CSA was included in least-squares analyses. The contribution of CSA to relaxation of the Gly-12 α-carbon was assumed to be negligible. Third, least-squares analysis of the Gly-12 Cα data was performed with and without the constraint that $\mathcal{S} = 1$. The latter is equivalent to the assumption that the motion of this backbone ^{13}C label can be adequately described by a single correlation time. However, it is reasonable to suppose, certainly for the random coil peptides, that the peptide chain must have substantial segmental flexibility, especially at glycine residues (Deslauriers et al., 1977). The mobility of the Gly-12 residue should therefore be better described in terms of its local motion superimposed on the diffusive motion of the entire peptide chain. Not surprisingly, lower χ^2 values and more consistent motional parameter values were obtained for the synthetic peptides when $\mathcal{S}$ was not constrained.

Finally, using a least-squares fitting procedure with a small number of experimental measurements has the potential problem of yielding misleading values for the motional parameters if even a single relaxation value is inaccurate. A graphical representation of $\mathcal{S}$, τ_e, and τ_m values consistent with T_1 and NOE data obtained at a single spectrometer frequency was found not only to obviate the problem of T_2 uncertainty but also to be an excellent means of evaluating peptide dynamics when limited data are available. This approach has the benefit of allowing one to obtain a range of $\mathcal{S}$ and τ_e values consistent with all physically plausible τ_m values and to visually compare $\mathcal{S}$ and τ_e trends across various samples.

(1) Dynamics in Dimethyl Sulfoxide/Water Mixtures. Least-squares-derived dynamics were remarkably similar for each of the synthetic peptides in 90% DMSO/10% D_2O (Table III). In this relatively viscous solvent, the peptides were expected to be essentially devoid of secondary structure. The NMR-derived least-squares τ_m values of 8.5–14.7 ns agree well with the overall rotational correlation time of 10.2 ns calculated for hydratd random coil melittin in this solvent.

Insight into the range of $\mathcal{S}$ and τ_e values describing Trp side-chain mobility is gained by examining $\mathcal{S}(\tau_m)$ and $\tau_e(\tau_m)$ plots generated from T_1 and NOE data. In Figure 5, $\mathcal{S}$ and τ_e were calculated for physically plausible τ_m values ranging from 1 to 20 ns. The similarity in the dynamics of the Trp side chain of each peptide over this range of τ_m values is apparent. Interestingly, the functional form of the $\mathcal{S}(\tau_m)$ plot constrains the order parameter to values of 0.55–0.85, inclusively, for all of the peptides *regardless* of the chosen τ_m value. Within the narrower τ_m range delimited by the 5.9- and 10.2-ns values predicted for the nonhydrated and hydrated random coil monomers in this solvent (see above), τ_e is constrained to 0.11–0.33 ns, while the range of allowed order parameter values narrows to 0.68–0.85.

The least-squares results for the Gly-12 α-carbon suggest that its mobility is only slightly more limited than that of the Trp side chain in this solvent. Over the τ_m range examined, T_1–NOE curves show that the Gly-12 Cα order parameter cannot fall below 0.6 for any of the peptides (Figure 5). For τ_m between 5.9 and 10.2 ns, the order parameter is confined to 0.75–0.95. Effective correlation times for Cα motion, however, are not usefully constrained (0.08–1.2 ns) due to the steep slope of the $\tau_e(\tau_m)$ plots.

(2) Dynamics in Water/Methanol Mixtures. Titration of MLT-W19 with methanol (CD_3OD) was carried out in an effort to detect changes in the Trp side-chain or peptide backbone mobility coincident with α-helix formation. Relaxation data obtained for the Trp Cδ_1 and Gly-12 Cα of monomeric MLT-W19, MLT-W17, and MLT-W11 in water/methanol solutions are compiled in Table II. The effect of methanol on the dynamics of MLT-W19 tetramer was also investigated.

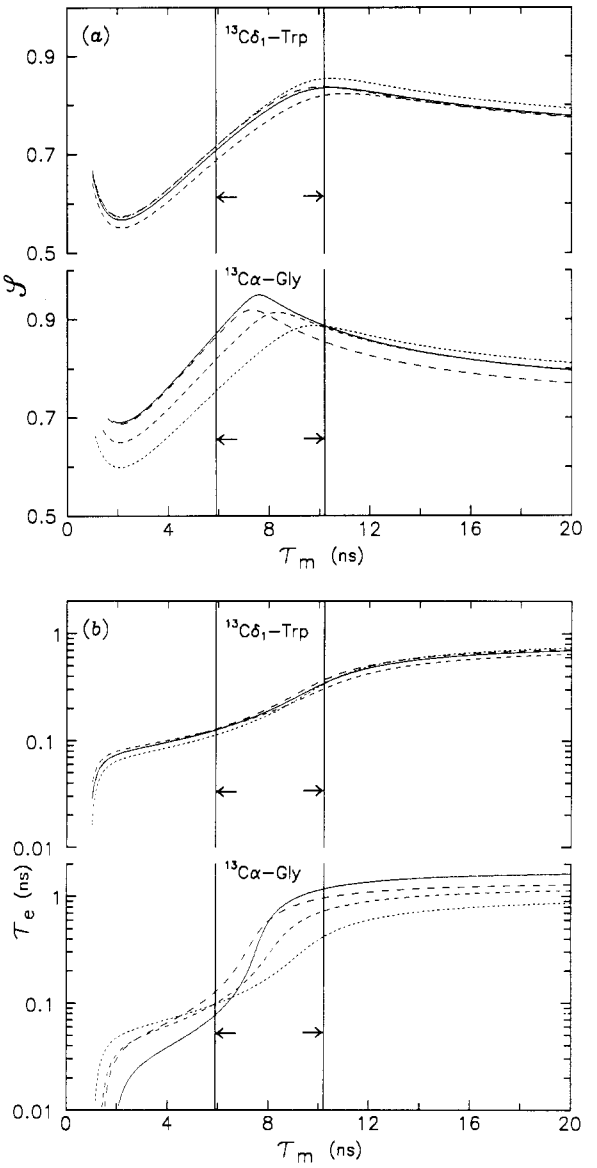

FIGURE 5: T_1–NOE curves generated from ^{13}C NMR relaxation data obtained at 75.4 MHz (Table II) displaying allowed values for the order parameter ($\mathcal{S}$) (a) and effective correlation time (τ_e) (b) of the [$^{13}C\delta_1$]Trp and [$^{13}C\alpha$]Gly labels as a function of the overall correlation time (τ_m) for MLT-W19, MLT-W17, MLT-W11, and MLT-W9 in 90% DMSO-d_6/D_2O. MLT-W19 (—); MLT-W17 (– –); MLT-W11 (- - -); MLT-W9 (···). Regions delimited by arrows indicate the range of overall correlation times (5.9–10.2 ns) predicted for the peptide monomers in this solvent. These curves were generated by MODLFREE using $n = 1$, $r_{CH} = 1.09$ Å, and $\Delta\delta = 200$ ppm, with [$^{13}C\delta_1$]Trp T_1 and NOE data; and $n = 2$, $r_{CH} = 1.10$ Å, and $\Delta\delta = 0$ ppm, with [$^{13}C\alpha$]Gly T_1 and NOE data.

The least-squares results, given in Table III, predict overall correlation times of 6.3–9.8 ns for monomeric melittin and 9.9–13.6 ns for melittin tetramer. The least-squares τ_m values give no evidence for methanol-induced dissociation of the tetramer, and the monomer τ_m values are essentially unchanged from those observed for these species in D_2O (see below). Although the predicted τ_m values of 3.0 and 5.5 ns for nonhydrated and hydrated α-helical melittin monomer, respectively, are less than values observed experimentally, the latter must be interpreted cautiously in light of the short

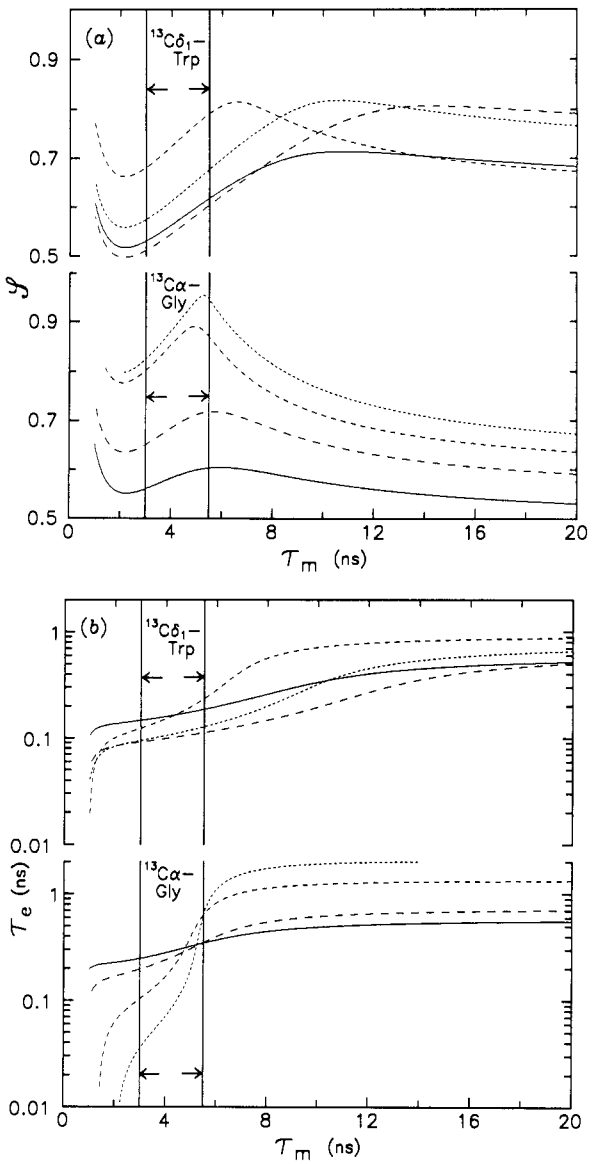

FIGURE 6: T_1–NOE curves generated from ^{13}C NMR relaxation data obtained at 75.4 MHz (Table II) displaying allowed values for the order parameter ($\mathcal{S}$) (a) and effective correlation time (τ_e) (b) of the [$^{13}C\delta_1$]Trp and [$^{13}C\alpha$]Gly labels as a function of the overall correlation time (τ_m) for MLT-W19 in D_2O/CD_3OD solutions. 0% CD_3OD (—); 10% CD_3OD (– –); 20% CD_3OD (- - -); 30% CD_3OD (···) (v/v). Regions delimited by arrows indicate the range of overall correlation times (3.0–5.5 ns) predicted for α-helical melittin monomer in this solvent. MODLFREE parameters are as stated for Figure 5.

spin–spin relaxation times. Even shorter T_2 values all but preclude a meaningful interpretation of least-squares motional parameters derived from Gly-12 Cα data. In this case, T_1–NOE curves provide a preferable means of interpreting the NMR data.

The lack of an obvious trend in least-squares $\mathcal{S}$ and τ_e values for the Trp-19 side chain as a function of methanol content is borne out by examination of the corresponding T_1–NOE curves in Figure 6. For τ_m values between 3.0 and 5.5 ns, the Trp side-chain order parameter takes on values of 0.51–0.80, while the effective correlation time for indole ring motion is constrained to 0.09–0.25 ns. Compared with the dynamics observed for the Trp side chain in DMSO, the rate and amplitude of indole ring motion are increased in water/methanol solutions, the former by a factor roughly equal to the relative viscosity of the solvents.

T_1–NOE curves indicate a marked change in local motion of the Gly-12 α-carbon in response to the addition of methanol to monomeric MLT-W19 (Figure 6). Assuming that the peptides remain monomeric and therefore retain similar overall correlation times in the various water/methanol mixtures, order parameters for Gly-12 Cα increase steadily with methanol content ($\mathcal{S}$ = 0.58 → 0.91, at τ_m = 4.3 ns), while the corresponding τ_e values fall (τ_e = 0.30 → 0.09 ns, at τ_m = 4.3 ns). A similar phenomenon is observed for motion of the Trp side-chain mobility upon formation of melittin tetramer (see below).

Relaxation data were also obtained for MLT-W17 and MLT-W11 in the presence of 30% CD_3OD (Table II). As noted for MLT-W19, least-squares τ_m values were larger than expected for α-helical monomers. T_1–NOE curves (not shown) suggested that the mobility of the Trp-11 side chain may be slightly greater than that of Trp-17 or Trp-19, while Gly-12 Cα mobility in the analogues was essentially identical with that observed for MLT-W19 in this solvent.

(3) Dynamics in Aqueous Solutions. Relaxation data collected for samples of MLT-W19, MLT-W17, and MLT-W11 in salt-free D_2O are compiled in Table II. Data could not be obtained for a concentrated salt-free sample of MLT-W11 (6.45 mM) or MLT-W9 (any concentration) in D_2O presumably due to peptide aggregation resulting in broad-line ^{13}C NMR spectra. Results of least-squares analyses are presented in Table III.

Although it was thought initially that the monomeric form of MLT-W19 would predominate at concentrations slightly higher than 4 mM in aqueous solutions of low ionic strength and acidic pH (Lauterwein et al., 1980), MLT-W19 was found to remain monomeric only at concentrations $<\sim$1 mM in salt-free D_2O (see preceding paper in this issue). However, relaxation data were collected for tetrameric MLT-W19 (6.17 mM) in D_2O containing 0.05–1 M NaCl. Each of the dilute peptide samples ($\sim$1 mM) for which relaxation data had been collected in salt-free solution was also titrated with NaCl. In the case of MLT-W19 (1.11 mM), relaxation data could not be obtained for the Gly-12 Cα resonance since this peak was split in each of the NaCl-containing samples resulting in low signal to noise ratios (see preceding paper in this issue). However, satisfactory data were obtained for monomer- and tetramer-predominant samples of MLT-W19 in salt-free D_2O.

Correlation times of 2.8 and 4.8 ns were predicted above from the solvent-accessible surface area of nonhydrated and hydrated random coil monomer, respectively. The discrepancy between the experimental least-squares τ_m value of 8.7 ns for MLT-W19 monomer value and the predicted range of τ_m values (2.8–4.8 ns) is most likely due to error in the measured T_2 value, although other explanations are possible (see Discussion). T_1–NOE curves generated from Trp-19 Cδ_1 and Gly-12 Cα relaxation data, shown in Figure 7, illustrate distinctive Trp-19 dynamics in melittin monomer and tetramer. For τ_m between 2.8 and 4.8 ns, Trp-19 side-chain motion is characterized by an order parameter of 0.52–0.59 and an effective correlation time of 0.14–0.17 ns. For Gly-12 α-carbon motion, one finds $\mathcal{S}$ = 0.55–0.59 and τ_e = 0.23–0.30 ns over this same range of τ_m values. It is worth noting, however, that due to the functional form of the Gly-12 Cα $\mathcal{S}(\tau_m)$ plot, essentially no limits need be placed on τ_m for monomeric MLT-W19 in order to constrain the α-carbon order parameter to a relatively narrow range of values.

For melittin tetramer, least-squares analyses of Trp-19 Cδ_1 data yielded τ_m values ranging from 10.1 to 12.4 ns, irrespective of NaCl concentration. By comparison, τ_m values derived from Gly-12 Cα relaxation data varied from 8.9 to 11.3 ns. These experimental results are in accord with the

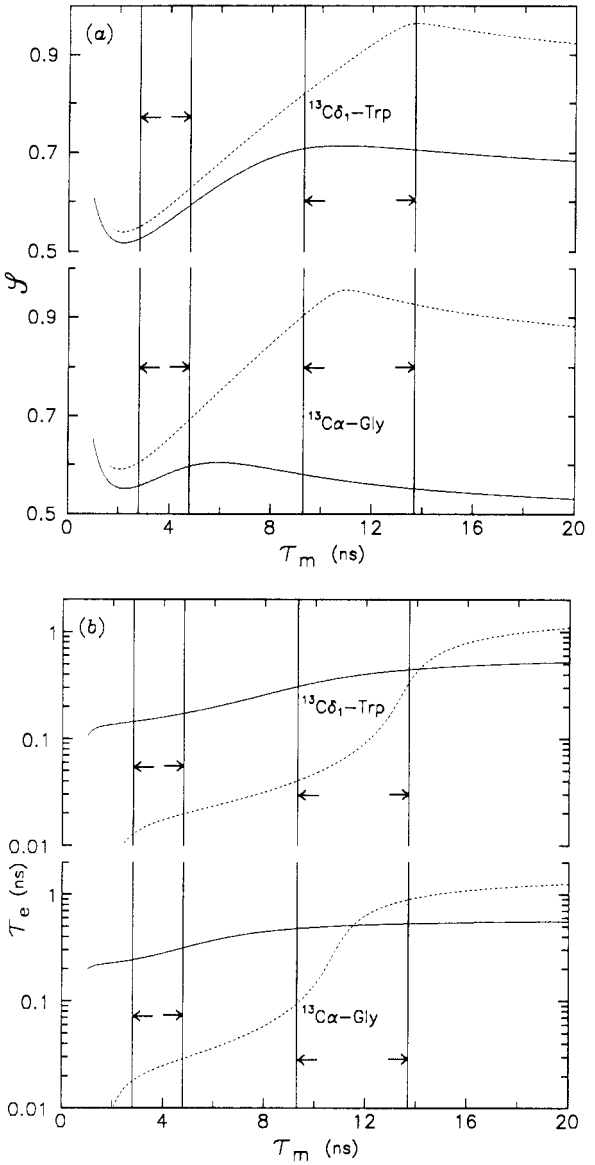

FIGURE 7: T_1–NOE curves generated from ^{13}C NMR relaxation data obtained at 75.4 MHz (Table II) displaying allowed values for the order parameter ($\mathcal{S}$) (a) and effective correlation time (τ_e) (b) of the [$^{13}C\delta_1$]Trp and [$^{13}C\alpha$]Gly labels as a function of the overall correlation time (τ_m) for MLT-W19 monomer (1.11 mM) (—) or tetramer (6.17 mM) (---) in D_2O. Regions delimited by arrows indicate the range of overall correlation times predicted for unstructured melittin monomer (2.8–4.8 ns) and for melittin tetramer (9.3–13.7 ns) in D_2O. MODLFREE parameters are as stated for Figure 5.

predicted values of 9.3 and 13.7 ns for the nonhydrated and hydrated tetramer.

As one might expect, titration of tetrameric MLT-W19 with NaCl had little effect on Trp-19 side-chain mobility (Table III). Assuming that the dynamics are similar in each of the samples of MLT-W19 tetramer, this series of experiments afforded the opportunity to statistically evaluate the derived motional parameters. The mean and standard deviation of motional parameter values collected for six samples of tetrameric melittin were found to be $\mathcal{S} = 0.89 \pm 0.04$, $\tau_e = 0.101 \pm 0.044$ ns, and $\tau_m = 10.72 \pm 0.77$ ns.

Between the predicted τ_m values of 9.3 and 13.7 ns for the tetramer, T_1–NOE curves (Figure 7) yield $\mathcal{S}$ values of 0.82–0.96 and τ_e values of 0.03–0.38 ns for Trp-19 $^{13}C\delta_1$; least-squares $\mathcal{S}$ and τ_e values fall within these ranges. While the larger order parameter for the Trp side chains of the tetramer is assured by the functional form of the $\mathcal{S}(\tau_m)$ plot, the steep slope of the $\tau_e(\tau_m)$ plot for MLT-W19 tetramer does not allow a similar conclusion in regard to the relative τ_e values for indole ring motion in the monomer and tetramer. However, the least-squares motional parameters extracted from several sets of relaxation data support the notion that the Trp-19 side chain moves more rapidly, yet with a smaller amplitude, in the tetramer than in the monomer.

Least-squares motional parameter values determined for the Gly-12 α-carbon demonstrated no readily interpretable trends. T_1–NOE curves, however, suggest that Gly-12 Cα mobility is more constrained in the tetramer with $\mathcal{S} = 0.91$–0.95 and $\tau_e = 0.09$–0.90 ns, while in the monomer $\mathcal{S} = 0.55$–0.59 and $\tau_e = 0.23$–0.30 ns (Figure 7).

In summary, changes in the NMR-derived motional parameters that accompany tetramer formation are as follows: (a) the overall correlation time τ_m *increases*; (b) the Trp-19 Cδ_1 order parameter *increases*; (c) the correlation time for Trp-19 side-chain motion *decreases*; and (d) the Gly-12 Cα order parameter *increases*.

Relaxation data were obtained for both salt-free and NaCl-containing samples of MLT-W17. Least-squares analysis of Trp-17 Cδ_1 relaxation data revealed a τ_m of 6.5 ns for the presumedly monomeric species and 10.4 ns at higher peptide concentration in D_2O (Table III). On addition of NaCl, τ_m increased from 6.5 to 9.0 ns, and then to 43.7 ns. Compared with MLT-W19, these τ_m values suggest that increases in NaCl or peptide concentration promote self-association, resulting in progressively longer overall correlation times. Although τ_m values for two of these samples are similar to that of MLT-W19 tetramer, it should not be inferred that this analogue forms a tetramer, or, for that matter, any structurally stable oligomer; nonspecific peptide aggregation is equally plausible. Indeed, in contrast to MLT-W19, the very large τ_m observed for MLT-W17 in 1 M NaCl implies that addition of salt only promotes the formation of increasingly larger aggregates.

Least-squares analysis of MLT-W17 Cδ_1 data reveals that indole ring motion in this monomeric melittin analogue is similar to Trp side chain motion in MLT-W19 under like conditions. T_1–NOE curves generated from Trp-17 δ_1-carbon relaxation data (not shown) also indicate that the mobility of the Trp side chain is nearly identical in monomeric MLT-W17 and MLT-W19. In the more concentrated salt-free sample of MLT-W17, $\mathcal{S}$ and τ_e both increase. This behavior contrasts with the *decreased* τ_e noted for the Trp-19 side chain under conditions where the tetramer predominates. In the presence of 0.5 M NaCl, however, Trp-17 side-chain mobility appears to resemble that of the Trp-19 side chain in tetrameric melittin. Overall, the Trp-17 side-chain dynamics suggest that this analogue does not form a stable, structurally defined oligomer at higher peptide concentrations or in the presence of NaCl. Moreover, in contrast to the motional behavior of the Gly-12 α-carbon(s) of MLT-W19 tetramer, the Cα order parameter of MLT-W17 does not increase, nor are larger τ_e values observed in either the NaCl-containing or concentrated salt-free samples of this analogue. This result is again consistent with the absence of a defined oligomeric structure for MLT-W17 under these sample conditions.

Relaxation data were obtained for MLT-W11 only at lower concentration (1.29 mM) in salt-free D_2O. Least-squares analysis of Trp-11 Cδ_1 data yielded order parameter and effective correlation time values that were quite similar to those noted above for monomeric MLT-W17 and MLT-W19. T_1–NOE curves (not shown) demonstrated that the amplitude of Trp-11 side-chain motion may be slightly less than that of Trp-19 or Trp-17, while having a slightly greater motional rate.

Table IV: Least-Squares Analysis of Combined Fluorescence and NMR Data Taken from Tables I and II for Comparable D_2O or D_2O/NaCl Samples[a]

	S	τ_e (ns)	τ_m (ns)
Monomers in Water			
MLT-W19[b]	0.56	0.159	4.0
MLT-W17[c]	0.56	0.146	3.5
MLT-W11[d]	0.58	0.091	3.3
Melittin Tetramer			
MLT-W19[e]	0.83	0.056	9.3

[a] For these calculations, $n = 1$, $r_{CH} = 1.09$ Å, $\Delta\delta = 200$ ppm, and $r_0(295\text{ nm}) = 0.175$. The estimated error in motional parameter values is ±15% (cf. Figure 1 caption). [b] Data taken from Table I, MLT-W19 (H_2O), and Table II, MLT-W19 (1.11 mM, D_2O). [c] Data taken from Table I, MLT-W17 (H_2O), and Table II, MLT-W17 (1.15 mM, D_2O). [d] Data taken from Table I, MLT-W11 (H_2O), and Table II, MLT-W11 (1.29 mM, D_2O). [e] Data taken from Table I, MLT-W19 (2 M NaCl), and Table II, MLT-W19 (average of T_1 and NOE values for six MLT-W19 tetramer samples: $T_1 = 0.261$ s, NOE = 1.28).

MLT-W11 Cα mobility also appeared to be comparable to that of dilute samples of MLT-W17 and MLT-W19 ($\sim$1 mM) in D_2O.

Combined Fluorescence and NMR Results. Least-squares analyses of combined fluorescence and NMR data were performed for monomeric MLT-W19, MLT-W17, and MLT-W11, as well as for MLT-W19 tetramer in water. Results are compiled in Table IV. Compared with the NMR-derived least-squares τ_m value of 8.7 ns for MLT-W19 monomer, the τ_m of 4.0 ns extracted from the combined analysis is in much better accord with values of 2.8 and 4.8 ns calculated from the solvent-accessible surface area of random coil melittin. The τ_m values determined for monomeric MLT-W17 and MLT-W11 also agree very well with the predicted overall correlation times. For tetrameric MLT-W19, the combined analysis τ_m value of 9.3 ns agrees exactly with the correlation time expected for the nonhydrated melittin tetramer and is also in good accord with the NMR-derived value of 10.7 ns. Order parameter and effective correlation time values of $S = 0.56 \pm 0.08$ and $\tau_e = 0.159 \pm 0.024$ ns, respectively, were found for the Trp-19 side chain of MLT-W19 monomer, compared with $S = 0.83 \pm 0.12$ and $\tau_e = 0.056 \pm 0.008$ ns for MLT-W19 tetramer. The Trp-17 and Trp-11 order parameters are comparable to that of MLT-W19 monomer, while the rate of Trp-11 side-chain motion is slightly greater than that of MLT-W17 or MLT-W19.

In general, motional parameter values determined by least-squares analyses of combined fluorescence and NMR data are less than values extracted from NMR data alone. However, the description of Trp side-chain motion that emerged from analysis of ^{13}C NMR relaxation data alone is corroborated in the combined analysis of steady-state fluorescence anisotropy, fluorescence lifetime, and NMR relaxation data. Specifically, the experimental result, that in melittin tetramer the amplitude of Trp side-chain motion lessens while its motional rate increases relative to that seen in the monomeric peptides, is again apparent.

Discussion

Overall Rotational Correlation Times. It is apparent that quantitation and interpretation of the rate and amplitude of internal motions depend critically on having a reasonably accurate value for the overall rotational diffusion rate of the macromolecule. This is often problematic since NMR experiments require protein concentrations 2–3 orders of magnitude greater than fluorescence studies. In the absence of concentration-dependent peptide aggregation, however, similar dynamics should be reported by both techniques. For random coil peptides and proteins, τ_m values derived from theory have shown good agreement with experiment (Brant & Flory, 1965a,b; Miller et al., 1967; Miller & Goebel, 1968); yet for small globular proteins, theoretical τ_m values are typically 2-fold less than observed values (Bauer et al., 1975; Massey & Churchich, 1979). In an attempt to resolve this problem, an empirical method of calculating τ_m from the solvent-accessible surface area of a macromolecule has been developed in this paper. By this method, overall rotational correlation times predicted for the various structural forms of melittin in aqueous solution are as follows (hydrated values are given parenthetically): random coil monomer, 2.8 ns (4.8 ns); α-helical monomer, 3.0 ns (5.5 ns); and melittin tetramer, 9.3 ns (13.7 ns). It is interesting that the correlation times expected for the unstructured and α-helical monomer are essentially the same. Also, the predicted τ_m value for the tetramer is only 2–3 times larger than that of the α-helical monomer, reflecting the displacement of solvent-accessible monomer surface area into helix–helix contacts within the solvent-inaccessible interior of the tetramer.

NMR-derived τ_m values of 6.5–8.7 ns (unstructured monomers), 6.3–9.8 ns (α-helical monomers), and 9.9–13.6 ns (melittin tetramer) compare favorably with the expected values. In particular, the predicted similarity between overall correlation times for the unstructured and α-helical monomeric species is observed experimentally. Although the experimental correlation times for the monomeric peptides are $\sim$1.5 times greater than values calculated for the hydrated molecules, it is interesting to note that NMR-determined diffusion coefficients for α-helical poly(L-lysine) and poly(L-glutamic acid) in water/organic solvent mixtures (Hanssum & Rüterjans, 1983; Hahn et al., 1985) predict correlation times of 8.0–9.2 ns for peptides with α-helical dimensions comparable to those of melittin[8]—the NMR-derived τ_m values for α-helical melittin in water fall within this range. On the other hand, τ_m values determined for the unstructured peptides in DMSO/D_2O ranged from 8.5 to 14.7 ns, which agree well with the expected value of 10.2 ns for hydrated random coil peptide monomers in this solvent system.

Possible sources of error in the experimental or predicted overall correlation time values include the following: (a) experimental error in determination of relaxation values; (b) uncertainty in the CSA contribution to relaxation of the Trp $^{13}C\delta_1$ label; (c) partial aggregation of the peptides in the NMR experiments; (d) electrostatic repulsion between positively charged C-terminal residues of melittin resulting in a greater persistence length for the random coil peptide—this effect would lengthen the expected overall correlation time; and (e) underestimation of protein hydration in calculations of expected τ_m values.

Increased τ_m values were noted for MLT-W17 and MLT-W11 in NaCl-containing solutions, and for MLT-W11 at high concentration in D_2O alone. In these cases, peptide aggregation is probably nonspecific. Overall correlation times for these analogues did not respond to increasing peptide or salt concentration in the discrete fashion exhibited by MLT-W19. Due to differences in peptide concentration between fluorescence and NMR samples, one must be wary of possible differences in the degree of peptide self-association as well as potential effects on internal dynamics. This is particularly true

[8] That is, for α-helical peptides having axial ratios between 3.0 and 4.0. These overall rotational correlation time values were calculated as $\tau_m = f/(6F_aD_a)$, where D_a is the experimentally determined rotational diffusion coefficient.

for NMR samples in which nonspecific aggregation was implicated. Thus, for concentrated or NaCl-containing samples of the melittin analogues, interpretation of motional parameters derived from combined analyses of fluorescence and NMR data is hazardous. However, since NMR data collected for melittin tetramer showed no evidence for more extensive peptide aggregation, a combined analysis is justifiable. Overall correlation times of 4.0 and 9.3 ns determined in this fashion for melittin monomer and tetramer, respectively, were in very good agreement with τ_m values calculated from solvent-accessible protein surface area.

Tryptophan Side-Chain Dynamics. Some generalizations can be made regarding the conformation and dynamics of MLT-W19 and analogues in DMSO and in D_2O (the latter at concentrations of $\sim$1 mM or lower). Under these conditions, motion of the Trp side chain appears to be essentially identical in all of the peptides; no significant differences in the rate or amplitude in indole ring motion were observed. Between the expected τ_m values of 5.9 and 10.2 ns for the unstructured monomers in DMSO, T_1–NOE curves predict order parameters of 0.65–0.85 and effective correlation times of 0.11–0.33 ns for indole ring motion (see Figure 5). For the corresponding expected τ_m values of 2.8–4.8 ns in D_2O, all of the peptides (excepting MLT-W9, which could not be studied due its poor solubility) again show similar Trp side-chain dynamics with $\mathcal{S}$ values of 0.52–0.59 and τ_e values of 0.14–0.17 ns. The mean correlation times for local motion of the Trp residue in DMSO and D_2O are in the ratio of the solution viscosity values (as are the overall correlation times), a result that emphasizes the important effect of solvent viscosity on the dynamics of solvent-exposed regions of protein structure. Finally, a combined analysis of fluorescence and NMR data for monomeric melittin yields motional parameter values of $S = 0.56 \pm 0.08$, $\tau_e = 0.159 \pm 0.024$ ns, and $\tau_m = 4.0 \pm 0.6$ ns. These values would appear to characterize Trp side-chain mobility in the absence of peptide secondary structure (cf. predceding paper in this issue). While the experimentally derived order parameter values might appear to be rather large for random coil peptides, it should be emphasized that the generalized order parameter pertains strictly to *local* motion of the Trp side chain (i.e., librational motion about side-chain α–β and β–γ bonds). Even for random coil polymers, constraints to side-chain mobility certainly exist; thus, apparently large $\mathcal{S}$ values are not untoward. Indeed, in the model for indole ring motion proposed below, the covalent geometry of the side chain dictates a minimum possible value for $\mathcal{S}$ of 0.36, which corresponds to complete rotational freedom about the β–γ bond.

In water/methanol mixtures, the mobility of the Trp side chain in the respective peptides does not change significantly with methanol content, nor do the dynamics differ much from those observed in D_2O alone (see Figure 6). This result is not surprising since solvent exposure and steric interactions of the Trp side chain would not be expected to be much different in the α-helical peptide than in the unstructured species. Although self-association of the melittin analogues alters Trp side-chain mobility, the observed changes follow no obvious pattern. For melittin itself, however, distinctive changes in indole ring motion do occur upon tetramer formation. From NMR data alone, indole ring and overall rotational motion of melittin tetramer are described by motional parameter values of $\mathcal{S} = 0.89 \pm 0.04$, $\tau_e = 0.101 \pm 0.044$ ns, and $\tau_m = 10.72 \pm 0.77$ ns. By comparison, analysis of combined fluorescence and NMR data collected for the tetramer reveal $S = 0.83 \pm 0.12$, $\tau_e = 0.056 \pm 0.008$ ns, and $\tau_m = 9.3 \pm 1.4$ ns. Contrasted with the unstructured monomer in water, indole ring motion in the tetramer is characterized by a shorter effective correlation time and an increased order parameter. The latter is intuitively consistent with increased steric constraints to Trp side-chain motion accompanying partial internalization of the indole moiety upon formation of the tetramer. The decreased effective correlation time implies a diminution in interactions of the indole moiety with solvent (i.e., collisions or hydration) that would otherwise attenuate the rate of motion of the solvent-exposed side chain.

Peptide Chain Dynamics. T_1–NOE curves suggest that the mobility of the Gly-12 α-carbon is quite similar for each of the synthetic peptides in DMSO solutions (see Figure 5). Moreover, Cα order parameters are only slightly larger than those observed for Cδ_1 of the Trp side chain. This observation is consistent with the presumed unstructured state of the peptide chain in this solvent. Between the expected τ_m values of 5.9 and 10.2 ns for the peptide monomers in DMSO, chain dynamics in the vicinity of the Gly-12 residue are characterized by order parameters of 0.75–0.95 and effective correlation times of 0.08–1.2 ns. The wide variation in τ_e values is a consequence of the steep slope of the $\tau_e(\tau_m)$ curve and also reflects the experimental uncertainty in τ_e at a given τ_m within this range. In contrast, in D_2O solutions, the effective correlation time for Gly-12 Cα motion is confined to 0.23–0.30 ns for τ_m values between 2.8 and 4.8 ns; order parameter values are similarly well defined ($\mathcal{S} = 0.55$–0.59).

The mobility of the Gly-12 α-carbon proved quite sensitive to methanol-induced changes in peptide backbone conformation. For τ_m values between 3.0 and 5.5 ns, T_1–NOE curves revealed larger order parameters and shorter correlation times for the Gly-12 Cα of MLT-W19 with increasing methanol content (see Figure 6). Similar α-carbon dynamics were observed for MLT-W17 and MLT-W11 in the presence of 30% methanol. The reduced amplitude and greater rate of peptide chain motion appear to coincide with the formation of a relatively more rigid structure (cf. Trp side-chain dynamics in melittin tetramer).[9] The data presented here indicate that the peptide chain dynamics of MLT-W19 and analogues change markedly even with partial (20–30%) α-helix formation.

The predominantly helical peptide chains of the tetrameric particle yield an order parameter for the Gly-12 Cα that approaches unity. Depending on the precise overall correlation time of the oligomer, the $\tau_e(\tau_m)$ plot demonstrates that the rate of α-carbon motion could be greater than or less than that of the monomer (see Figure 7). However, at the least-squares τ_m of 10.7 ns for the tetramer, τ_e is less than that obtained for the monomer. In any case, the mobility of the α-helical peptide chains of melittin tetramer is clearly distinct from that of the unstructured backbone. The dynamical changes observed in the present study would appear to complement the sensitivity of the Gly-12 Cα chemical shift to the helix–coil transition described in the preceding paper in this issue.

Model-Free Analysis of Combined Fluorescence and NMR Data. It should be emphasized that interpretation of motional parameters derived from combined fluorescence and NMR data must allow for potential problems associated with the relative sensitivity of the techniques. With current instrumentation and experimental procedures, a 2 order of magnitude difference in sample concentration is often required. Over this range of concentrations, substantial differences in

[9] In the preceding paper in this issue, CD and NMR spectra showed that the fractional helicity of MLT-W19 and analogues increases linearly with methanol content.

peptide dynamics might arise due to peptide aggregation. Hence, motional parameters at odds with those determined from NMR or fluorescence techniques alone might in part be due to the concentration variance. For this reason, motional parameters derived from combined analysis cannot be meaningfully interpreted for those samples of MLT-W17 or MLT-W11 which showed evidence of peptide aggregation by NMR (e.g., increased τ_m values). On the other hand, order parameter values derived from analysis of fluorescence or NMR data alone agreed well for samples in which the peptides were presumedly monomeric. One can infer from such results that a combined analysis of fluorescence and NMR data is then reasonable.

Similarly, since MLT-W19 tetramer occurs as a discrete species over a wide range of peptide concentrations and sample conditions appropriate to both fluorescence and NMR experiments, a combined analysis is justifiable. The agreement of order parameter values determined by fluorescence and NMR methods separately also appears to validate this approach. Indeed, the same conclusions regarding Trp-19 dynamics in melittin follow from analysis of combined fluorescence and ^{13}C NMR data as from either method alone. However, the combined approach does markedly improve agreement between predicted and observed τ_m values. Moreover, effective correlation times for Trp side-chain motion in the monomer (0.159 ns) and tetramer (0.056 ns) are, remarkably, identical with values of 0.16 and 0.06 ns, respectively, reported by Lakowicz et al. (1987) from time-resolved fluorescence anisotropy data. Together, these experimental results strongly support the physical validity of picosecond correlation times for Trp side-chain motion.

Clearly, more study into the appropriateness of combining fluorescence and NMR data to extract motional information is warranted. The observation in this work of an indole ring correlation time as short as 56 ps has important implications with regard to molecular dynamics calculations since this value is approximately within the time frame suggested for motion of the Trp side chain from such simulations (Levy, 1986; Axelsen et al., 1988). That the apparent correlation time is shorter for Trp side-chain motion in the tetramer than in the monomer is also an encouraging validation of assumptions that local motion of the fully solvent-exposed side chain may be slowed significantly by viscous drag. Side chains buried in the protein matrix might thus be expected to show a restricted amplitude but a greater rate of motion.

Physical Interpretation of Order Parameter Values. Given the experimental values for $\mathcal{S}$, it is possible to propose a model for motion of the Trp side chain and to place limits on the extent of that motion. Form Lipari and Szabo (1982a), the generalized order parameter can be written

$$\mathcal{S}^2 = \frac{4\pi}{5} \sum_{m=-2}^{2} |\langle C_{2m} \rangle|^2 \qquad (12)$$

where C_{2m} are the modified spherical harmonics of Brink and Satchler (1968), and the broken brackets ($\langle\ \rangle$) designate an equilibrium average within a macromolecule-fixed frame over all possible orientations of the $^{13}C\delta_1$–H bond that are accessible on a time scale shorter than the correlation time for overall reorientation of the macromolecule. The indole moiety of the Trp side chain can rotate about α–β and β–γ bonds. A situation whereby the planar aromatic ring moves only about the β–γ bond allows direct calculation of a flipping angle about this bond given an experimental order parameter value for motion of the Trp $^{13}C\delta_1$–H vector. If one assumes that any angle is equally probable in a range of $\pm\varphi_0$ about an equilibrium orientation, then it follows from eq 12 that

$$\mathcal{S}^2 = \frac{1}{4}(3\cos^2\theta_0 - 1)^2 + 3\left[\sin\theta_0 \cos\theta_0 \left[\frac{\sin\varphi_0}{\varphi_0}\right]\right]^2 + \frac{3}{16}\left[\sin^2\theta_0 \left[\frac{\sin(2\varphi_0)}{\varphi_0}\right]\right]^2 \qquad (13)$$

where θ_0 is the fixed angle between the $C\delta_1$–H vector and the β–γ bond, taken here to be 72.3° (Momany et al., 1975). This expression is equivalent to that derived by London and Avitabile (1978) in considering a specific model for relaxation in ^{13}C-labeled methionine.

For the MLT-W19 tetramer, the observed order parameter of 0.83 (±0.12) corresponds to a flipping angle of ±37° (19–51°) about the β–γ bond. Comparing this with the X-ray structure of the tetramer, in which the Trp-19 indole ring lies in a relatively constrained pocket defined by several apolar amino acid side chains, this estimate seems reasonable. In MLT-W19 monomer, an order parameter of 0.56 (±0.08) gives a flip angle of ±71° (60–90°). Any motion about the α–β bond would lead to a smaller flip angle about the β–γ bond for a given $\mathcal{S}$. Extension of this model to extract flip angles about both the α–β and β–γ bonds would require additional information regarding the orientational order of the Trp γ-carbon. Nonetheless, from experimental measurement of a generalized order parameter for the indole ring $^{13}C\delta_1$–H vector, plausible limits can be placed on the amplitude of Trp side-chain motion.

Conclusions. In this work, the model-free approach to analysis of ^{13}C NMR relaxation data has been expanded to allow the use of steady-state fluorescence anisotropy and lifetime data in selected systems. The availability of fluorescence data provides an excellent alternative to less precise T_2 measurements. In lieu of fluorescence or T_2 data, however, the use of T_1 and NOE data to construct $\mathcal{S}(\tau_m)$ and $\tau_e(\tau_m)$ plots offers an easily accessible and quantitative method of evaluating rapid local motions in proteins. The use of T_1–NOE curves also encourages the interpretation of side-chain dynamics in terms of a probable range of $\mathcal{S}$ and τ_e values as opposed to the calculation of "unique" values for these parameters from T_1, T_2, and NOE data obtained at a single spectrometer frequency.

The utility of the model-free approach in providing accurate quantitative information about rapid local motions in proteins is evident. Overall correlation times determined by these methods for melittin and melittin analogues agree well with values predicted on the basis of solvent-accessible protein surface area. In the case of melittin tetramer, motional parameters for the single Trp side chain verified the existence of spatially restrained motion which can be characterized by a flip angle of ±37° about the β–γ bond with a correlation time of 56 ps. In contrast, indole ring motion in the monomer is of greater amplitude with a flip angle of ±71° with a correlation time of 159 ps. The importance of these correlation times derives from their agreement with the results from time-resolved fluorescence anisotropy measurements and from the fact that the method described here provides an accessible alternative or complement to that technique. Further, the results support the existence of motions on the time scale predicted by molecular dynamics simulations. With advances in NMR techniques for measuring ^{13}C relaxation rates (e.g., ^{13}C to ^{1}H polarization transfer), fluorophores might not need to be selectively ^{13}C-labeled to achieve the benefits of the combined approach presented here.

Ongoing studies with other peptides and with larger proteins

will attempt to better correlate experimental results with molecular dynamics calculations. It will also be important to more precisely delineate the relative contributions of magnetic dipole–dipole, CSA, and other potential interactions to relaxation of ^{13}C-labeled fluorophores used in such studies. Further work on modification of the fluorescence and NMR expressions to allow for noncolinearity of the ^{13}C–H vector and the fluorescence dipoles as well as for nonaxially symmetric CSA is also in progress.

ACKNOWLEDGMENTS

We are indebted to B. D. Ray for assistance with NMR techniques. We thank K. E. Nollet for providing assistance with CHARMM. This paper is taken in part from the doctoral thesis of one of us (A.J.W.).

REFERENCES

Altenbach, C., & Hubbell, W. L. (1988) *Proteins 3*, 230–242.

Axelsen, P. H., Haydock, C., & Prendergast, F. G. (1988) *Biophys. J. 54*, 249–258.

Bauer, D. R., Opella, S. J., Nelson, D. J., & Pecora, R. (1975) *J. Am. Chem. Soc. 97*, 2580–2582.

Bevington, P. R. (1969) *Data Reduction and Error Analysis for the Physical Sciences*, Chapter 11, pp 204–246, McGraw-Hill, New York.

Branchini, B. R., Prendergast, F. G., Spencer, G. A., Hagdahl, J. D., Ray, B. D., & Kemple, M. D. (1987) *J. Labelled Compds. Radiopharm. 24*, 637–643.

Brant, D. A., & Flory, P. J. (1965a) *J. Am. Chem. Soc. 87*, 2788–2791.

Brant, D. A., & Flory, P. J. (1965b) *J. Am. Chem. Soc. 87*, 2791–2800.

Brink, D. M., & Satchler, G. R. (1968) *Angular Momentum*, Clarendon Press, Oxford.

Brooks, B. R., Bruccoleri, R. E., Olafson, B. D., Stotes, D. J., Savanirnathan, S., & Karplus, M. (1983) *J. Comput. Chem. 4*, 187–217.

Brown, E. M., Pfeffer, P. E., Kumosinski, T. F., & Greenberg, R. (1988) *Biochemistry 27*, 5601–5610.

Cantor, C. R., & Schimmel, P. R. (1980) *Biophysical Chemistry. Part II: Techniques for the Study of Biological Structure and Function*, Vol. II, Chapter 10, pp 539–590, W. H. Freeman, San Francisco.

Deslauriers, R., Levy, R. C., McGregor, W. H., Sarantakis, D., & Smith, I. C. P. (1977) *Eur. J. Biochem. 75*, 343–346.

Engel, L. W., & Prendergast, F. G. (1981) *Biochemistry 20*, 7338–7345.

Georghiou, S., Thompson, M., & Mukhopadhyay, A. K. (1982) *Biophys. J. 37*, 159–161.

Gratton, E., & Lopez-Delgado, R. (1980) *Nuovo Cimento Soc. Ital. Fis., B 56B*, 110–124.

Gratton, E., & Limkeman, M. (1983) *Biophys. J. 44*, 315–324.

Hahn, U., Hanssum, H., & Rüterjans, H. (1985) *Biopolymers 24*, 1147–1156.

Hanssum, H., & Rüterjans, H. (1983) *J. Chem. Phys. 78*, 4687–4697.

Henry, G. D., Weiner, J. H., & Sykes, B. D. (1986) *Biochemistry 25*, 590–598.

Heyn, M. P. (1979) *FEBS Lett. 108*, 359–364.

Hughes, L. T., Cohen, J. S., Szabo, A., Niu, C., & Matsuura, S. (1984) *Biochemistry 23*, 4390–4394.

Jähnig, F. (1979) *Proc. Natl. Acad. Sci. U.S.A. 76*, 6361–6365.

John, E., & Jähnig, F. (1988) *Biophys. J. 54*, 817–827.

Karplus, M., & McCammon, J. A. (1981) *CRC Crit. Rev. Biochem. 9*, 293–349.

Kawato, S., Kinosita, K., & Ikegami, A. (1977) *Biochemistry 16*, 2319–2324.

Kinosita, K., Kawato, S., & Ikegami, A. (1977) *Biophys. J. 20*, 289–305.

Lakowicz, J. R., Prendergast, F. G., & Hogan, D. (1979) *Biochemistry 18*, 520–527.

Lakowicz, J. R., Maliwal, B. P., Cherek, H., & Balter, A. (1983) *Biochemistry 22*, 1741–1752.

Lakowicz, J. R., Laczko, G., Gryczynski, I., & Cherek, H. (1986) *J. Biol. Chem. 261*, 2240–2245.

Lakowicz, J. R., Cherek, H., Gryczynski, I., Joshi, N., & Johnson, M. L. (1987) *Biophys. J. 51*, 755–768.

Lauterwein, J., Brown, L. R., & Wüthrich, K. (1980) *Biochim. Biophys. Acta 622*, 219–230.

Levy, R. M. (1986) *Ann. N.Y. Acad. Sci. 482*, 24–43.

Lipari, G., & Szabo, A. (1980) *Biophys. J. 30*, 489–506.

Lipari, G., & Szabo, A. (1982a) *J. Am. Chem. Soc. 104*, 4546–4559.

Lipari, G., & Szabo, A. (1982b) *J. Am. Chem. Soc. 104*, 4559–4570.

London, R. E., & Avitabile, J. (1978) *J. Am. Chem. Soc. 100*, 7159–7165.

MacKerell, A. D., Jr., Rigler, R., Nilsson, L., Hahn, U., & Sanger, W. (1987) *Biophys. J. 26*, 247–261.

Massey, J. B., & Churchich, J. E. (1979) *Biophys. Chem. 9*, 157–162.

McCain, D. C., Ulrich, E. L., & Markley, J. L. (1988) *J. Magn. Reson. 80*, 296–305.

Meiboom, S., & Gill, D. (1958) *Rev. Sci. Instrum. 29*, 688–691.

Miller, W. G., & Goebel, C. V. (1968) *Biochemistry 7*, 3925–3935.

Miller, W. G., Brant, D. A., & Flory, P. J. (1967) *J. Mol. Biol. 23*, 67–80.

Momany, F. A., McGuire, R. F., Burgess, A. W., & Scheraga, H. A. (1975) *J. Phys. Chem. 79*, 2361–2381.

Némethy, G., Peer, W. J., & Scheraga, H. A. (1983) *J. Phys. Chem. 87*, 1883–1887.

Parhami, P., & Fung, B. M. (1985) *J. Am. Chem. Soc. 107*, 7304–7306.

Perrin, F. (1934) *J. Phys. Radium 5*, 497–511.

Perrin, F. (1936) *J. Phys. Radium 7*, 1–11.

Petrich, J. W., Longworth, J. W., & Fleming, G. R. (1987) *Biochemistry 26*, 2711–2722.

Rice, D. M., Meinwald, Y.C., Scheraga, H. A., & Griffin, R. G. (1987) *J. Am. Chem. Soc. 109*, 1636–1640.

Rule, G. S., Pratt, E. A., Simplaceanu, V., & Ho, C. (1987) *Biochemistry 26*, 549–556.

Schmidt, P. G., Sierzputowska-Gracz, H., & Agris, P. F. (1987) *Biochemistry 26*, 8529–8534.

Shaka, A. J., Frenkiel, T., & Freeman, R. (1983) *J. Magn. Reson. 52*, 159–163.

Terwilliger, T. C., & Eisenberg, D. (1982a) *J. Biol. Chem. 257*, 6010–6015.

Terwilliger, T. C., & Eisenberg, D. (1982b) *J. Biol. Chem. 257*, 6016–6022.

Tran, C. D., & Beddard, G. S. (1985) *Eur. Biophys. J. 13*, 59–64.

Veeman, W. S. (1984) *Prog. Nucl. Magn. Reson. Spectrosc. 16*, 193–235.
Weaver, A. J., Kemple, M. D., & Prendergast, F. G. (1988) *Biophys. J. 54*, 1–15.
Weaver, A. J., Kemple, M. D., & Prendergast, F. G. (1989) *Biochemistry* (preceding paper in this issue).
Weiner, J. H., Dettman, H. D., Henry, G. D., O'Neil, J. D. J., & Sykes, B. D. (1987) *Biochem. Soc. Trans. 15*, 81–85.

Structural and Functional Analysis of NADPH-Cytochrome P-450 Reductase from Human Liver: Complete Sequence of Human Enzyme and NADPH-Binding Sites†

Mitsuru Haniu,*,‡ Michael E. McManus,§ Donald J. Birkett,§ Terry D. Lee,‡ and John E. Shively‡
Division of Immunology, Beckman Research Institute of the City of Hope, Duarte, California 91010, and Department of Clinical Pharmacology, School of Medicine, Flinders University of South Australia, Bedford Park 5042, Australia
Received March 29, 1989; Revised Manuscript Received June 28, 1989

ABSTRACT: The complete amino acid sequence of human liver NADPH-cytochrome P-450 reductase has been determined by microsequence analysis and mass spectrometry. The total sequence consists of 676 amino acids initiated by an amino-terminal acetyl group. There is no evidence for posttranslational modifications, including Asn-linked glycosylation. The human enzyme exhibits sequence homology in the range of 92–95% with other mammalian enzymes. Sequence differences were mainly confined to several hydrophilic regions in the NH_2-terminal and COOH-terminal domains. Since the human enzyme is immunochemically distinct from the rabbit enzyme despite similar enzymatic properties, it is likely that these variable hydrophilic regions are potential antigenic determinants. The NADPH-depleted enzyme is inactivated by either fluorescein isothiocyanate, a lysine-specific reagent, or 5-(iodoacetamido)fluorescein, a cysteine-specific reagent. In both cases, protection by NADP(H) prevents enzyme inactivation by the reagents. Isolation of fluorescent peptide from 5-(iodoacetamido)fluorescein-inactivated enzyme identified Cys 565 as the specifically NADPH-protected residue.

The flavoprotein NADPH-cytochrome P-450 reductase (EC 1.6.2.4) is an integral component of the cytochrome P-450 xenobiotic metabolizing system (Williams, 1976; Schwab & Johnson, 1987). This enzyme system is found in both hepatic and extrahepatic tissues (McManus et al., 1987a; Hall et al., 1989) and is localized in the endoplasmic reticulum and nuclear membrane of cells (Kasper, 1971). Together with cytochrome P-450, NADPH-cytochrome P-450 reductase is essential for reconstitution of xenobiotic metabolizing activity in purified systems. The reductase functions by catalyzing electron transfer from NADPH to the hemoprotein during catalysis (Lu & West, 1978). In addition to providing reducing equivalents to cytochrome P-450, the reductase is also involved in electron transfer from NADPH to heme oxygenase (Yoshida & Kikuchi, 1978) and cytochrome b_5 (Ilan et al., 1981). The reductase has been purified from a variety of eucaryotic and procaryotic tissues (McManus et al., 1989) including human liver (Guengerich et al., 1981; Abraham et al., 1986; McManus et al., 1987a, 1989) and placenta (Osawa et al., 1981; Muto & Tan, 1986). By contrast with cytochrome P-450, which is comprised of a family of isozymes, only one form of NADPH-cytochrome P-450 reductase has been identified in each species investigated, and in the mouse, this enzyme is located on chromosome 6 (Simmon et al., 1985). Each form of NADPH-cytochrome P-450 reductase isolated has been shown to contain one molecule each of FAD and FMN per polypeptide chain. A cDNA for rat reductase was cloned by Gonzalez and Kasper (1982), while Black and Coon (1982) published protein sequence data on rabbit reductase. Since then, the amino acid sequence of pig liver reductase has been reported from protein sequence analysis (Haniu et al., 1984, 1986; Vogel et al., 1985; Vogel & Lumper 1986), and the cDNA-deduced sequences of the rat enzyme (Porter & Kasper, 1985; Murakami et al., 1986), rabbit enzyme (Katagiri et al., 1986), and yeast enzyme (Yabusaki et al., 1988) have been reported. Partial sequence of trout enzyme has been also reported (Urenjak et al., 1987). The amino acid sequence homology between the pig, rat, and rabbit enzymes is approximately 90%.

Except for two reports giving the amino acid composition (Muto & Tan, 1986; McManus et al., 1989), no structural information on the human NADPH-cytochrome P-450 reductase is available. However, indirect evidence from immunological studies suggest that there are structural differences between human reductase and its animal counterparts (Guengerich et al., 1981; Osawa et al., 1981; McManus et al., 1989). The reductase contains two prosthetic groups, FAD and FMN, and interacts with NADPH, cytochrome P-450, cytochrome b_5, and cytochrome *c*, suggesting the presence of up to six binding domains on the molecule (Porter & Kasper, 1986; Nisimoto, 1986). Since important binding regions on enzymes such as NADPH-cytochrome P-450 reductase exhibit sequence conservation across species, determination of the amino acid sequence of the human reductase is an important first step in understanding its structure–function relationships. We have therefore determined the complete amino acid sequence of the human NADPH-cytochrome P-450 reductase

† This work was supported by NIH Grants GM 34426 and CA 33572.
* To whom correspondence should be addressed.
‡ Beckman Research Institute of the City of Hope.
§ Flinders University of South Australia.

0006-2960/89/0428-8639$01.50/0